



Norwegian University of
Science and Technology

Influence of siderophore-iron
complexation on the growth of the diatom
Skeletonema costatum: a mass
spectroscopy approach

Claire Katja Peterson

Environmental Toxicology and Chemistry

Submission date: May 2016

Supervisor: Murat Van Ardelan, IKJ

Norwegian University of Science and Technology
Department of Chemistry

Abstract

The growth of the diatom *Skeletonema costatum* was monitored using *in vivo* fluorescence under concentration gradients of desferrioxamine B (DFB) and enterobactin to test the siderophores' effect on iron bioavailability. Changes in the composition of dissolved organic matter, including the added siderophores, were then identified using HPLC-MS. Samples for organic matter analysis were taken once when the diatom reached exponential growth in all siderophore conditions.

Previous research into the effect of siderophores on algal growth has indicated positive or negative growth of the diatom depends on both the diatom species and the type of siderophore. In this project, DFB inhibited growth at first, but eventually the diatom entered exponential phase growth even at the highest concentration of added DFB, 10 μ M. Enterobactin showed less concentration dependent limitation of iron bioavailability and in lower concentrations showed an increase in growth compared to the control. The findings suggest that its ability to act as an iron scavenger in seawater is inhibited by its hydrophobicity.

From compound ions found using MS, a range of potential iron chelators was detected. The siderophores were successfully identified along with DFB's complex with iron, ferrioxamine. Potential DFB metabolites matched predicted mass to charge ratios and chemical formulas but could not be confirmed structurally by the MS databases used. Saccharides, potential iron chelators released by algae, were also discovered. In the DFB series, the abundances of compound ions were significantly different based on the concentration of siderophore in the sample.

The results of this project represent a snapshot of the dissolved organic matter present in samples. Further experiments tracking siderophores along with a few known chelators throughout diatom growth would enhance understanding of the role of chelators in diatom iron uptake. HPLC-MS is a promising technique to uncover the relationship between iron chelators and diatoms.

Acknowledgements

Many thanks to my supervisor, Murat Ardelan, for the thesis opportunity and for always being enthusiastic about all things related to iron in the oceans.

Also thanks to Nicolas Sanchez for the advice and support, Susana Villa Gonzalez for the amazing help with MS, and Kåre Kristiansen for taking over the MS project and running last minute samples

Table of Contents

List of Figures.....	ix
List of Tables.....	xi
Abbreviations.....	xiii
1 Introduction	1
1.1 Marine Iron Sources and Biogeochemistry	1
1.2 Siderophores.....	4
1.3 Bacteria and Diatom Interactions.....	6
1.4 Objectives.....	8
2 Theory.....	9
2.1 DFB & Enterobactin	9
2.2 Detecting Siderophores with Mass Spectroscopy.....	10
3 Experimental Methods.....	13
3.1 Cleaning	13
3.2 Seawater Collection	13
3.3 Algal Growth Conditions	14
3.4 Experimental Setup	14
3.5 Solid-Phase Extraction of DOM.....	16
3.6 UPLC-MSE Method	17
4 Data Analysis using Progenesis QI	19
4.1 Chromatogram Alignment.....	19
4.2 Experimental Design	19
4.3 Peak Picking.....	20
4.4 Deconvolution	20
4.5 Compound Identification	21
4.6 Compound Statistics	21
5 Results and Discussion	25
5.1 Algal growth	25
5.2 DFB Series	27
5.2.1 Compound Ions Discovered.....	27
5.2.2 Identifying DFB and Ferrioxamine.....	27
5.2.3 PCA	30
5.2.4 Potential DFB Metabolites.....	33
5.2.5 Non-DFB Related compounds	36

5.3 Enterobactin Series.....	37
5.3.1 Compound Ions Discovered.....	37
5.3.2 Identifying Enterobactin.....	37
5.3.3 PCA	39
5.3.4 Non-Enterobactin Related Compounds.....	40
5.4 Comparing DFB and Enterobactin	41
5.5 Future work.....	43
6 Conclusion	45

Bibliography

Appendix

List of Figures

Figure 1. The nitrogen cycle showing metal cofactors. Adapted from Morel et al. 2003. ¹⁹	3
Figure 2. Depth profiles of nitrate and dissolved iron. Reproduced from Johnson et al. 1997, each profile represents a measurement at a different experimental station. ²¹	4
Figure 3. The main siderophore functional groups.	5
Figure 4. Redox potentials for Fe-complexes with varying ligands. Reproduced from Dhungana et al. 2005. ²⁶	6
Figure 5. DFB and its iron complex.....	9
Figure 6. Enterobactin complexed with iron (left) and un-complexed (right).....	10
Figure 7. Electrospray process in positive mode. Photo taken by Andreas Dahlin.	11
Figure 8. Q-TOF mass spectrometer designed by Waters. Reproduced from the Waters website.	12
Figure 9. Experimental setup.	15
Figure 10. Overview of the SPE procedure. Reproduced from Lucci et al., licensee InTech 2012.....	17
Figure 11. Example loadings plots with variables (represented by dots) negatively correlated (a), positively correlated (b), and not correlated (c).....	22
Figure 12. <i>in vivo</i> fluorescence, 441/82 nm excitation, of DFB samples.....	25
Figure 13. <i>in vivo</i> fluorescence, 441/82 nm excitation, of enterobactin samples	26
Figure 14. Mass spectrum of a 10000 nM DFB experimental sample.	28
Figure 15. Fragmentation spectrum for DFB	29
Figure 16. Mass spectrum highlighting ferrioxamine at 614 m/z and its iron isotopic pattern.....	29
Figure 17. PCA from DFB samples. Compound ions corresponding to DFB (4.30_561.3616m/z) and ferrioxamine (2.95_614.2710m/z) are highlighted in red.	Error! Bookmark not defined.
Figure 18. Abundance profile for DFB. From left to right: 10 nM, 500 nM, 10000 nM, noAlgae 500 nM, colors correspond to those on the PCA.	31
Figure 19. Abundance profile for ferrioxamine. From left to right: 10 nM, 500 nM, 10000 nM, noAlgae 500 nM, colors correspond to those on the PCA.	31

Figure 20. Degradation of DFB by the bacteria <i>Azospirillum irakense</i> . Reproduced from Winkelmann et al. ⁵¹	344
Figure 21. DFB fragmentation from collision induced tandem MS (adapted from Groenewold et al.) ⁵⁴	35
Figure 22. Enterobactin peak at 670 m/z	38
Figure 23. Fragmentation of the identified enterobactin molecule.	38
Figure 24. Enterobactin PCA with the enterobactin compound (9.81_670.1525m/z) highlighted.....	39
Figure 25. Enterobactin Abundance Profile From left to right: 0.01 nM, 0.5 nM, 50 nM, noAlgae 0.5 nM, colors correspond to those on the PCA.....	40

List of Tables

Table 1. Potential chelators discovered in the DFB series.....	27
Table 2. Potential chelators discovered in the enterobactin series.	37

Abbreviations

ANOVA	Analysis of Variance
CO ₂	Carbon Dioxide
DFB	Desferrioxamine B/Deferoxamine
DOM	Dissolved Organic Matter
ESI	Electrospray Ionization
Fe	Iron
HNLC	High Nitrate Low Chlorophyll
HPLC	High Performance Liquid Chromatography
ICP	Inductively Coupled Plasma
Q-TOF	Quadrupole Time of Flight
LDPE	Low Density Polyethylene
MS	Mass Spectroscopy
m/z	Mass to Charge
OM	Organic Matter
PC	Principal Component
PCA	Principal Component Analysis
SPE	Solid Phase Extraction

1 Introduction

1.1 Marine Iron Sources and Biogeochemistry

Atmospheric dust is the major source of new iron to the open ocean.^{1,2} Global maps of aerosol iron distribution from the Sea-Air Exchange Program in the Pacific³ and the Atmosphere-Ocean Chemistry Experiment in the North Atlantic⁴ show that the major dust flux areas in the North Pacific and North Atlantic correspond to regions near arid land. In the Southern Ocean, which has high nitrate low chlorophyll (HNLC) waters, less dust flux is present.

Sediments are also a major source of nutrients. Research into the transport of iron in the Southern Ocean has identified shelf sediments as a main source of iron.^{5,6} Horizontal flux transports shelf-derived nutrients due to the Antarctic Circumpolar Current interacting with continental shelf waters. Iron is also derived from vertical flux, which brings nutrients to surface waters in upwelling regions, where currents transport deep water to the surface.⁶ Other new sources of iron include iceberg and glacial melt, volcanoes, and hydrothermal vents.¹

The chemical form of iron in the oceans is determined by filtrate size and divided into dissolved and particulate. Dissolved iron can pass through a 0.2 or 0.4 μm filter while particulate iron is retained.⁷ Dissolved iron contains both the soluble species as well as a substantial fraction of colloidal.¹ Distribution of iron between the chemical forms depends on redox reactions, complexation with inorganic and organic ligands, and scavenging. Complexation by ligands can keep iron in a dissolved form while scavenging involves the conversion of dissolved iron to particulate forms through adsorption and precipitation.¹

Both dissolved and particulate forms of iron are important for marine organisms in surface waters. A large portion of particulate iron is remineralized and reused.⁷ It has been estimated that around 80% of iron uptake in the euphotic zone in the equatorial Pacific is a result of regeneration while the rest is a result of external iron sources.⁸

Although iron is the fourth most abundant element in the Earth's crust, dissolved iron concentrations in the surface waters of the open ocean are relatively low.⁹ However, these concentrations of around 0.2 nM^1 are larger than the theoretical predicted concentration minimum of 0.01 nM^{10} , which takes into account the solubility of the hypothetical dominant iron species based on surface water conditions.

Dissolved iron exists in two oxidation states, Fe(II) and Fe(III), either freely or complexed with inorganic or organic ligands. Redox reactions between these species take place throughout the water column.¹¹ In surface waters, due to the presence of oxygen and a pH of around 8, iron is most prevalent as thermodynamically stable, oxidized Fe(III) in a particulate iron oxyhydroxide form with low solubility.¹² The higher experimental measurements of dissolved iron in surface waters are most likely due to increased iron solubility as a result of complexation with organic ligands. Two classes of ligands have been established. Strong ligands (L1) are primarily found in surface waters and include those produced by bacteria as a technique to obtain iron. The other class of weak ligands (L2) is found throughout the water column and is made up of degradation products from bacteria breaking down organic matter. Both classes are thought to play a large role in keeping iron soluble.¹

There has been debate about which redox form is most useful for biota. Fe(II) is directly soluble in water and is thought to be the most biologically available form, making up about 50% of the dissolved iron concentrations in surface waters.⁹ Fe(II) is supplied to the upper ocean by photo-reduction of Fe(III) and from aerosols coming to ocean surfaces with iron in the Fe(II) form, probably due to photochemical reactions and an acidic environment as the dust is transported.² Fe(II) prefers sulfur and nitrogen ligands often found in enzymes, whereas Fe(III) prefers oxygen ligands.¹³ However, it has been suggested that enzymes on the cell surfaces of phytoplankton are able to reduce iron that can then be used by the cell.¹⁴ This indicates that primary producers can uptake either the reduced (Fe(II)) or oxidized (Fe(III)) forms of iron.

The first wave of research into the interaction between iron and phytoplankton came as a result of John Martin, who hypothesized in 1989 that new primary productivity is limited by iron in HNLC zones of the ocean.¹⁵ In these areas, concentrations of nitrate and phosphate macronutrients are high, but phytoplankton growth is low.⁹ This could be explained by limited iron bioavailability. If iron concentrations were increased in these areas, phytoplankton growth rates would also increase. A rise in phytoplankton biomass has the capacity to reduce atmospheric and surface water carbon dioxide (CO₂) levels through photosynthetic uptake of CO₂ and consecutive removal of CO₂ to the deep ocean as the remains of organisms sink to the bottom.¹⁵ Subsequent iron-enrichment experiments carried out in both lab settings¹⁶ and the open ocean¹⁷ have confirmed a link between iron and phytoplankton growth, though iron is one of many factors.

Iron influences the marine nitrogen cycle by playing a role in both nitrate/nitrite reduction and nitrogen fixation. Large changes in the nitrogen budget can be linked to changes in iron deposition. This is a result of iron's role in nitrogen fixation, which brings new nitrogen into the marine cycle through the conversion of N_2 supplied from the atmosphere into biologically usable forms, NO_3 , NO_2 , or NH_3 .¹⁸ As shown in the nitrogen cycle in Figure 1, it is a cofactor in nitrite and nitrate reductase, which reduce the nitrate and nitrate forms, as well as nitrogenase, which is an enzyme that reduces N_2 to NH_3 .¹⁹

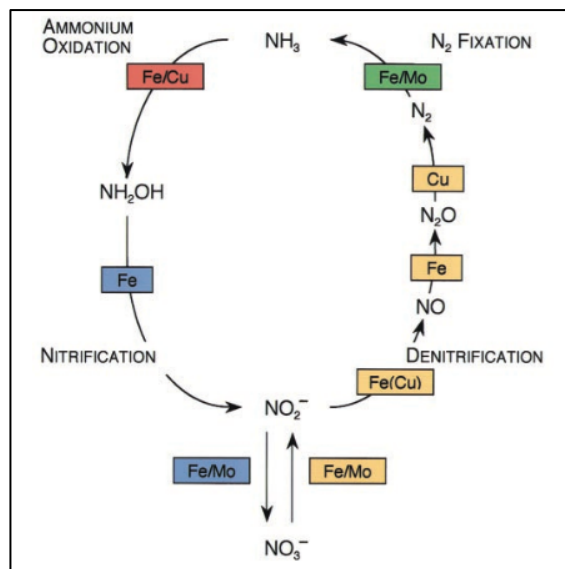


Figure 1. The nitrogen cycle showing metal cofactors. Adapted from Morel et al. 2003.¹⁹

It has been suggested that about 75% of the world's oceans have iron-limited nitrogen fixation, particularly due to the *Trichodesmium* cyanobacteria found in tropical and subtropical oceans.²⁰ These cyanobacteria contain the nitrogenase enzyme, which has one iron protein and one iron-molybdenum protein. Nitrogen fixation produces NH_3 , which is used as a nitrogen source for most phytoplankton. However, the larger species such as diatoms rely on NO_3 to maintain growth rates. This nitrogen species requires more iron to generate after fixation, in its reduction from NH_3 .¹⁹

Iron's role in the nitrogen cycle affects the carbon cycle by providing a macronutrient needed for primary production, increasing organic matter in the upper ocean. It also primarily influences the carbon cycle through its role in photosynthesis and respiration, functioning as an electron transporter in both processes.¹⁹ This effect is highlighted in its depth profile, showing low concentrations at the surface and higher concentrations in deep waters. In surface waters, primary producers use it to create organic matter, and in deeper waters,

bacteria break down this organic matter, releasing CO₂ and iron. This type of profile is similar to that of other known nutrients including nitrate (Figure 2).²¹ Therefore, iron is linked to the production of new carbon in the marine system.

New carbon also affects the biological carbon pump, which is the transport of organic matter out of the euphotic zone.²² With more organic matter produced at the surface, there is more particulate organic matter that will sink to the deep ocean, where it is converted back into CO₂ and sequestered.²² The heavier phytoplankton such as diatoms with silica outer layers are most likely to sink to the deep ocean and require more iron to produce.

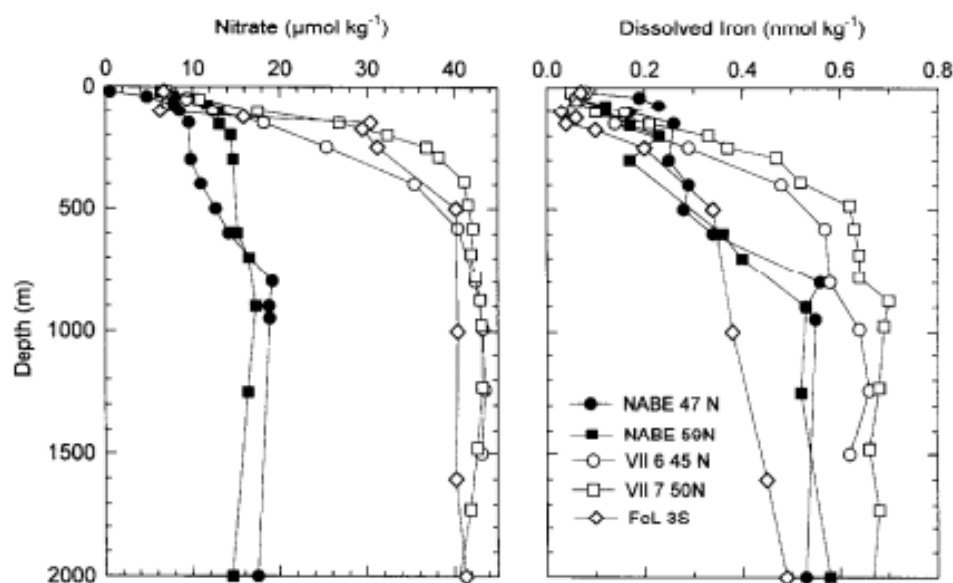


Figure 2. Depth profiles of nitrate and dissolved iron. Reproduced from Johnson et al. 1997, each profile represents a measurement at a different experimental station.²¹

1.2 Siderophores

Organic complexation of iron makes up about 99% of all dissolved iron in seawater.⁹ The upper portion of the water column has an excess of ligands, which consist largely of the strong L1 class. Some of these ferric chelators are siderophores produced by bacteria under iron-limited conditions to keep iron in solution.^{1,23} They have a low molecular weight and are highly selective for Fe(III).²⁴ Siderophores are also produced in soil and other systems by bacteria and fungi. They are most often classified based on their Fe-coordinating functional groups. The three most common are catechols, hydroxamic acids, and α -hydroxy-carboxylic acids (Figure 3).²⁵ Chelation relies on the oxygen atoms.

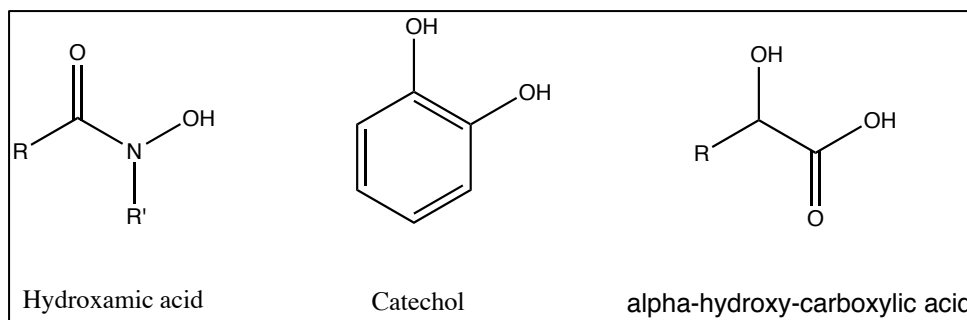


Figure 3. The main siderophore functional groups.

Siderophore structure determines how soluble the iron-siderophore complex is, and thus, how much iron is kept in solution in excess of Fe(III) hydroxide solubility. Cyclic structures show a greater affinity for Fe(III) than linear molecules.²⁴ Denticity describes the number of iron-binding functional groups, and most siderophores are hexadentate since Fe(III) has six coordination sites. Higher denticity correlates with higher stability of the Fe complex.²⁴ This stability is shown by redox potentials, which measure how easily a compound accepts electrons.²⁴ The greater the potential, the greater the affinity for electrons and the more easily the molecule is reduced. Hexadentate siderophores show more negative potentials than tetradentate ligands, indicating they are more stable.²⁴

Siderophore affinity for Fe(III) is a result of the strong Lewis acid nature of Fe(III), which seeks out hard donor atoms like oxygen to accept its electrons. This forms a strong bond between ligand and metal. Fe(II) is a softer metal center that likes more polarizable ligands such as nitrogen.²⁴ Fe(III) complexes have more negative redox potentials than Fe(II) complexes relative to the aquo ion, and these Fe(II) complexes are readily oxidized to Fe(III) complexes.²⁶ Redox potential values, however, are dependent on the presence of competing chelators and the competition of H⁺ ions as a result of pH.²⁴ An overview of the redox potentials of Fe-complexes is shown in Figure 4.

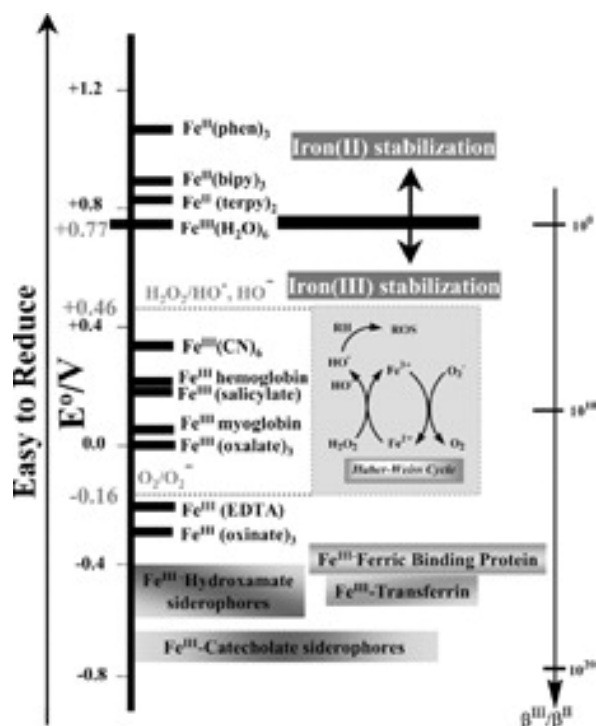


Figure 4. Redox potentials for Fe-complexes with varying ligands. Reproduced from Dhungana et al. 2005.²⁶

Many siderophores have been identified as naturally occurring in the marine environment. In 2008, Ferrioxamine E and G, both hydroxamate type siderophores, were identified in the Atlantic Ocean.²⁷ Iron-chelating compounds with catechol and hydroxamic acid groups have also been detected off the coast of New Zealand²⁸ and California²⁹. High performance liquid chromatography mass spectroscopy (HPLC-MS) was used to identify the siderophore functional groups.

1.3 Bacteria and Diatom Interactions

Diatoms are a type of photosynthetic eukaryote at the bottom of the marine food chain. They are responsible for about 20% of photosynthetic activity, and thus make a large amount of the organic matter present in the oceans.³⁰ Their characteristic silica shells cause them to sink when they die, pulling organic carbon into the deep ocean, affecting the biological pump. Bacteria, on the other hand, feed on the organic carbon produced by the diatoms, converting it back into CO_2 .³⁰ Diatoms and bacteria are closely related; every algal cell has a phycosphere, which describes the area outside the cell where bacteria grow due to released cell products. They have coexisted for millions of years, developing complex interactions that affect biogeochemical cycles within the oceans.³⁰

Looking at the iron biogeochemical cycle, many marine bacteria produce siderophores.³⁰ Eukaryotic phytoplankton have not been found to produce siderophores; however, they release mono and polysaccharides that weakly bind iron. Bacteria living in the phycosphere can also access the iron bound in these saccharides.³⁰ Iron-based interactions between the bacteria in the phycosphere and diatoms have formed as they compete for this essential nutrient.

Bacteria produce siderophores as a result of quorum sensing, in which they release small molecules to signal other cells. If diatoms are able to recognize these molecules as precursors to siderophores, they could increase their iron assembling power. Some diatoms acquire iron from organic ligands by reducing Fe(III) to Fe(II) by a cell surface ferric reductase followed by oxidation back to Fe(III) with a multicopper oxidase. It has been proposed that the molecules released by bacteria in quorum sensing supply copper for the latter enzyme.³⁰

Another example of diatoms acquiring iron from bacterially produced ligands comes from research into the iron complex vibrioferrin, produced by gammaproteobacteria often found associated with algae. Siderophores with α -hydroxy acid functional groups are more photolabile than other classes. Vibrioferrin is in this class and has a high photosensitivity.^{30,31} When exposed to light, Fe(III) is reduced to Fe(II), which is readily oxidized in marine conditions back to Fe(III). This free iron molecule is then bioavailable to phytoplankton. The supply of soluble Fe(III) to algal cells is hypothesized to come in exchange for organic carbon released by the diatoms for bacterial use.³⁰

Previous experiments testing the effect of siderophores on diatom growth have given mixed results. In a study testing *Thalassiosira oceanica* in the presence of iron bound to the siderophore desferrioxamine B, a positive effect on growth was seen due to the ability of the diatom to reduce organic ligand bound Fe(III) on the cell surface.³² Another study using the same siderophore showed a decrease in iron bioavailability and a decrease in the growth of several diatoms including *Thalassiosira antarctica*.³³ A study by Strzepak et al., which examined the effect of low iron conditions and siderophores on the growth rate of many Southern Ocean diatoms, found that the ability to grow in the presence of iron bound to strong organic ligands was species dependent.³⁴ For species unable to uptake iron bound to siderophores, increasing concentrations of siderophore have been shown to decrease iron bioavailability.³⁵

1.4 Objectives

Based on previous experiments performed at NTNU, cultured algae under controlled iron concentration conditions with large amounts of siderophores present in the system initially showed no growth but eventually began to grow. This was hypothesized to be a result of the siderophores structurally changing over the course of the experiment, allowing more iron to become bioavailable to the algae, and/or the algae releasing chelators or structurally adapting to acquire iron from the siderophores.

This master's project attempts to identify these new chelators and/or structural changes in two siderophores, DFB and enterobactin, using HPLC-MS. Samples were taken during an experiment monitoring the growth of the diatom *Skeletonema costatum* with varying levels of siderophore concentration. It makes up part of a larger experiment studying the interaction between iron and organic ligands and the effect on growth and physiology of a diatom phytoplankton species under controlled conditions.

The general objectives are:

- (1) To grow microalgae under gradients of two different siderophores, testing for the effect on iron bioavailability
- (2) To identify changes in the DOM composition (including the added siderophores) using HPLC-MS

2 Theory

2.1 DFB & Enterobactin

Desferrioxamine B, also known as deferoxamine or DFB, is part of the widely studied hydroxamic acid group and is easily available. When complexing with iron, the hydroxylamine group (-NOH) loses a proton, and iron is stabilized by bonds formed with the carbonyl and hydroxylamine groups (Figure 5). It is an example of a hexadentate ligand with an affinity for Fe(III) which is about 20 orders of magnitude higher than for Fe(II).²⁴ Ferrioxamine B, DFB's iron complex, has been found in seawater and is excreted by a species of marine bacteria.³⁶ Studies on how it influences iron bioavailability have shown both positive effects on the growth of diatoms in the presence of the iron-siderophore complex and also cases of negative effects.³²⁻³³

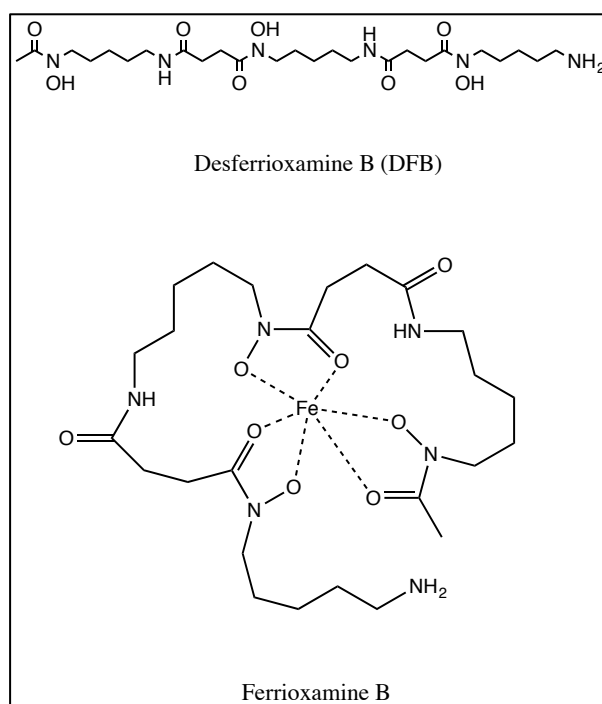


Figure 5. DFB and its iron complex.

Enterobactin is also a hexadentate ligand with a larger solubility constant (K_{sol}) than DFB, indicating it dissolves Fe(III) more efficiently.²⁴ DFB has a $\log(K_{sol})$ of 6.83 while enterobactin has a value of 14.62.²⁴ It also has a larger proton independent stability constant for the Fe(III) bound complex with 10^{49} for enterobactin compared to $10^{30.6}$ for DFB.³⁷ Iron is bound through catechol side chains (Figure 6). In general, as shown by the redox potentials in

Figure 4, catechol-Fe(III) complexes are more stable, or less likely to be reduced, than hydroxamate-Fe(III) complexes such as DFB. The complexes' stability is thought to be due to the rigidity of the metal cavity and hydrogen bonding.³⁸ Enterobactin is widely used as an iron chelator in the medical field. For example, it is found in many iron dietary supplements.

Both siderophores are strong and specific iron chelators, but represent different classes based on their functional groups. This could affect their degradation in the presence of algae or their competition with iron chelators produced by algae.

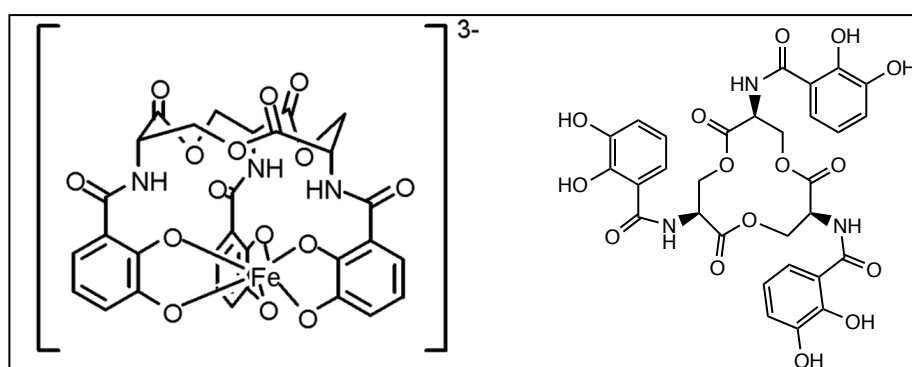


Figure 6. Enterobactin complexed with iron (left) and un-complexed (right).

2.2 Detecting Siderophores with Mass Spectroscopy

High-performance liquid chromatography (HPLC) – electrospray ionization (ESI) mass spectroscopy (MS) has become the method of choice for siderophore detection, particularly for hydroxamic acid-type siderophores.^{36,27} HPLC can separate compounds in a liquid sample based on polarity. In reversed phase chromatography, hydrophobic molecules adsorb onto a hydrophobic solid support in a polar aqueous mobile phase. Adding a more organic solvent decreases the polarity and reduces the hydrophobic interaction between the solute and the solid support resulting in desorption. More hydrophobic molecules have a longer retention time on the solid support and require a larger amount of organic solvent to desorb.³⁹ In other words, the more polar molecules will elute first with the polar aqueous phase while nonpolar molecules will be retained longer and elute once the mobile phase becomes less polar, i.e. has more organic solvent.

The separated compounds are then ionized and converted to the gas phase before entering the MS. In the ESI method, voltage is applied between a capillary and a counter electrode creating an electric field (Figure 7). The sample liquid is continuously passed through the capillary creating a mist of charged droplets as they encounter the electric field.

As these droplets pass towards the MS, they go down a pressure and potential gradient, evaporating the solvent. A stream of nitrogen drying gas often helps this process. Finally, the electric field within the droplet allows the ion to be ejected into the gas phase.⁴⁰ These ions then pass into the MS where they are separated and detected. This method has good sensitivity at low detection limits.³⁶

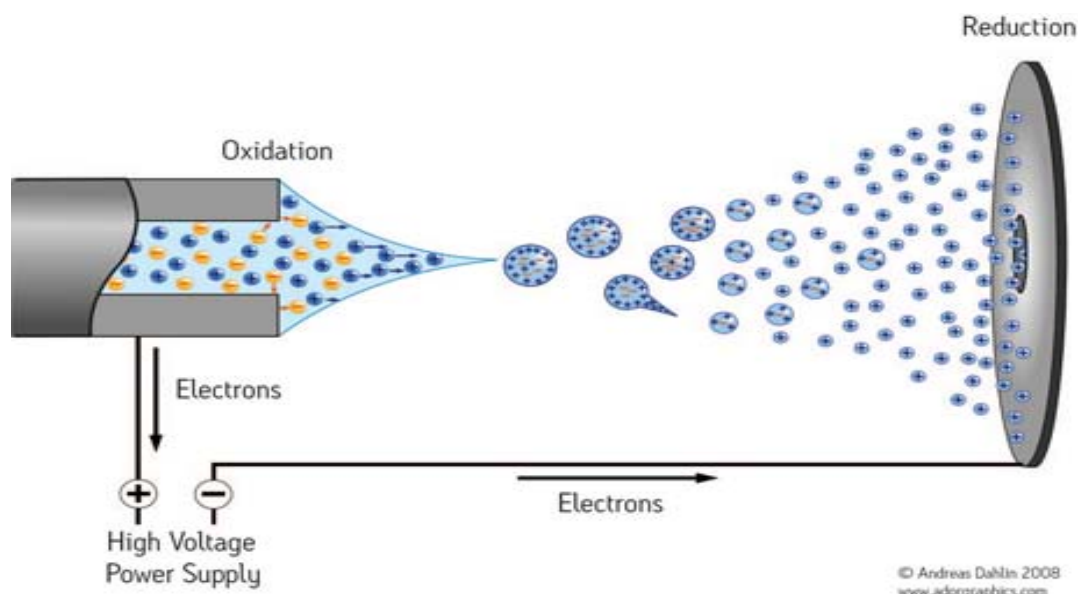


Figure 7. Electro spray process in positive mode. Photo taken by Andreas Dahlin.

Many mass analyzers are hybrid systems such as the Quadrupole and Time-of-Flight (Q-TOF) system, which is known for high mass accuracy and resolution (Figure 8). After ionization, ions pass through a quadrupole, which consists of four parallel rods with a direct current potential between them. This acts as an ion guide during MS and an ion filter in MS/MS.⁴¹ A high voltage pulse then accelerates ions into the TOF drift tube, where a reflectron is often used to increase the length.⁴² All ions exit the source with the same potential from the pulse and all similarly charged ions have similar kinetic energies (KE). They can then be separated by mass. The smaller the mass, the higher the velocity as

$$KE = \frac{1}{2}mv^2,$$

where m = mass and v = velocity.

The time it takes for the ion to pass from the ion source to the detector is measured. The ion's velocity is equal to the known length of the path divided by the calculated time. This velocity is then inversely proportional to the square root of the mass as shown by

$$v = \frac{d}{t} = \left(\frac{2KE}{m}\right)^{\frac{1}{2}},$$

where d = path length, t = time, KE = kinetic energy, and m = mass.⁴² Lower m/z ions will reach the detector first.

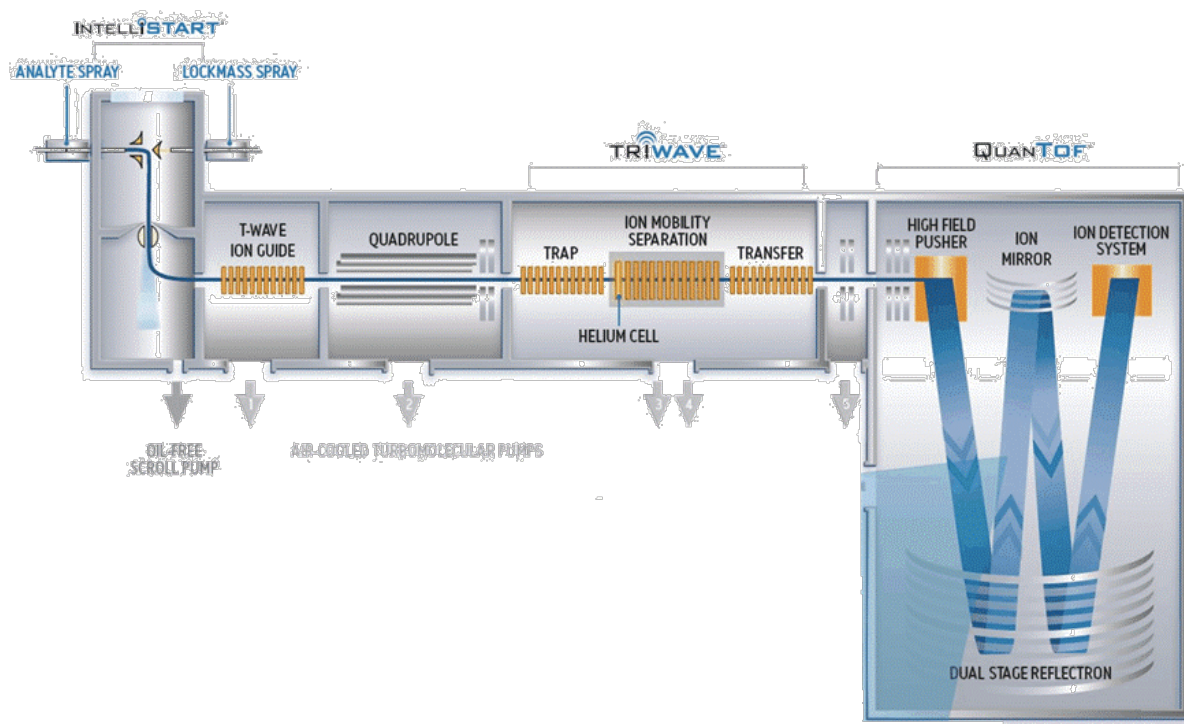


Figure 8. Q-TOF mass spectrometer designed by the Waters Corporation™. Reproduced from the Waters website.

ESI is a soft ionization technique, meaning it is less likely to fragment molecules during ionization. Further fragmentation is often used to help confirm the identity of siderophores and reveal structural information that could help classify unknown siderophores. The Waters™ MS^E system contains a collision cell, which rapidly alternates between high and low energy. This gives precursor ion information along with fragmentation data for that ion.⁴³ Along with fragmentation data and precursor ion data, isotopes are used to identify compounds in MS. The two most abundant iron isotopes, ⁵⁴Fe and ⁵⁶Fe, have been used to identify the presence of bound iron in siderophores.⁴⁴

While ESI-MS is the qualitative method of choice, inductively coupled plasma mass spectroscopy (ICP-MS) is often used to quantify iron bound siderophores.⁴⁵ However, since ICP is a hard ionization technique, the organic part of the molecule is destroyed and no structural information can be obtained.⁴⁶ Quantification is only based on the metal content and cannot be performed for the un-complexed siderophore.⁴⁶

3 Experimental Methods

3.1 Cleaning

Before the experiment, all bottles, tubing and other lab instruments were cleaned by trace metal analysis standards to prevent iron contamination. All low-density polyethylene (LDPE) bottles were soaked in a super detergent solution for several days then rinsed with Milli Q water. This was followed by washing with methanol overnight and another rinsing with Milli Q. Then, 3.5 M nitric acid was added for several days followed by another rinsing with Milli Q. Ultra Pure 0.5 M nitric acid was then added to the bottles which were left to soak for about a week. Finally, the bottles were rinsed with Milli-Q. Nitric acid and Milli-Q water were also used to clean pipette tips and tubing. Items were dried in a Class 1000 cleanroom and were then kept double plastic bagged until use. AirClean Systems Laminar Flow workstations (Class 100) were used during siderophore additions.

3.2 Seawater Collection

In November 2015, seawater was collected from 100 m deep in the Trondheim fjord using the seawater intake valve at the Trondheim Biological Station located at 63° North in Trondheim, Norway. For the experiment, 80 L were filtered through acid washed filters (0.45 +0.2 μm Sartorius Sartobran 300) into 20 L LDPE bottles. Another 90 L was collected for UPLC/MS method development for the detection of dissolved organic matter in seawater. This water was vacuum filtered through pre-combusted GF/F filters (0.2 μm Whatman). The filtered water was then transferred from glass flasks to 20 L compressible LDPE bottles. All flasks and bottles for these 90 L had been pre-rinsed with methanol. Water wasn't autoclaved, leaving a natural bacterial abundance.

Ion exchange resin (Chelex-100 Bio-Rad Laboratories) was added in excess to the 20 L bottles of filtered water, which were placed on shakers for two days. The water was then passed through an acid-washed Poly-prep Chromatography column with a built-in polyethylene frit (100-300 μm pore size, Bio-Rad Laboratories). The column contained approximately 4 mL Chelex-100 slurry per column. This Chelex-100 removed most labile iron and other trace metals to known background concentrations. Known amounts of trace metals were then added as described in the next section.

3.3 Algal Growth Conditions

The experiment was performed in a climate-controlled room kept at 14°-15°C and 40-60% humidity. There was 24 hour fluorescent lighting with a mean luminous intensity of 78 $\mu\text{mol m}^{-2} \text{s}^{-1}$. The *Skeletonema costatum* species used was a NIVA-BAC 36 strain culture collection algae from Norsk Institutt for vannforskning (NIVA). The strain was maintained in normal f/2 medium. The experiment was conducted in EDTA/metal ion buffered seawater media based on the revised Aquil artificial algal culture medium.⁴⁷ Macronutrients (nitrate, phosphate, and silicate) were kept as independent stocks and were individually passed through Chelex-100 containing columns. The trace metal solution was prepared with an EDTA concentration of 10 μM , and each metal's concentration was adjusted to keep the free ion concentrations described in Price et al.⁴⁷

To adapt the microalgae to the growth conditions, 1 mL aliquots were transferred from the original f/2 medium to the low iron growth medium (LIGM). The inoculum added to the experiment corresponded to the 3rd batch culture (exponential phase) in LIGM. Deferoxamine mesylate salt (1 g, $\geq 92.5\%$ TLC, Sigma) and enterobactin (E3910, 1 mg, Sigma) were used as the siderophores for the experiment. Iron concentrations were not manipulated during the course of the experiment. The amount of background Chelex-100 labile iron was measured and quantified with ICP-MS to be 1.2 ± 0.5 nM for the samples.

3.4 Experimental Setup

Small, 500 mL, bottles with a wide range of concentrations accompanied larger, 4 L, bottles with the lowest, middle, and highest concentrations. Only the larger bottles were taken for organic matter analysis and were used to ensure a large amount of organic material. An outline of the experimental setup is shown in Figure 9.

400 mL of culture were added to each of 36 plastic 500 mL bottles. 18 bottles were placed on one half of the shelving in the climate controlled room and 18 on the other, separating the DFB from the enterobactin samples. Of each set of 18 bottles, 3 acted as controls only containing algae culture and no siderophore. The other 15 contained triplicates of 5 concentrations of siderophore. For DFB, these concentrations were 10 nM, 50 nM, 500 nM, 2500 nM, and 10000 nM. Lower concentrations of enterobactin were used: 0.01 nM, 0.05 nM, 0.5 nM, 2.5 nM, and 50 nM. These lower concentrations were a result of limited supply of the compound due to the high price.

Another 24 four-liter LDPE bottles were added for organic matter analysis, 12 for each siderophore. These contained three liters of culture. Each series contained triplicates of the lowest, middle and highest concentrations of siderophore along with three control bottles. Each control bottle contained the middle concentration of siderophore but no algae. These controls were designed to show how the siderophores were affected by the culture medium including any degradation that could occur without the presence of algae.

DFB Series						
0.5 L Culture Bottles	10 nM	50 nM	500 nM	2500 nM	10000 nM	Control (no siderophore)
4 L Culture Bottles	10 nM	500 nM	10000 nM	Control (500 nM siderophore, no algae)		
Enterobactin Series						
0.5 L Culture Bottles	0.01 nM	0.05 nM	0.5 nM	2.5 nM	50 nM	Control (no siderophore)
4 L Culture Bottles	0.01 nM	0.5 nM	50 nM	Control (0.5 nM siderophore, no algae)		

Figure 9. Experimental setup.

All final siderophore concentrations were achieved after five equivalent additions, one addition every second day throughout the course of the experiment.

In vivo chlorophyll fluorescence was monitored to track growth of the algae. The ability of chlorophyll to fluoresce makes this an appealing parameter to track during the course of the experiment. If more fluorescence is observed, more chlorophyll is present, and photosynthetic activity is also expected to be high. This assumes that fluorescence positively correlates to the absorption of visible light in the photosystems responsible for capturing energy for photosynthesis.⁴⁸

Fluorescence was measured with a Turner designs Trilogy laboratory fluorometer. Using this data, the large bottles were sampled for organic material once those with the highest concentration of siderophore began to show signs of chlorophyll fluorescence and all samples showed exponential growth. The experiment lasted 13 days.

3.5 Solid-Phase Extraction of DOM

From the Chelex-100 treated seawater collected for MS method development, three 10 L bottles contained only seawater, another three contained seawater with 10000 nM DFB, and another three contained seawater with 50 nM enterobactin. Dissolved organic matter (DOM) was extracted from these bottles. From the experiment, DOM was also extracted from the large experimental bottles: 2 bottles from each of the low, middle, and high siderophore concentrations.

Following the procedure from Dittmar et al. 2008, solid phase extraction (SPE) of DOM was carried out.⁴⁹ The SPE cartridges (Agilent Bond Elut PPL) used contained columns of a modified styrene divinylbenzene polymer, PPL, sorbent (Figure 10). This PPL sorbent retains molecules with a wide range of polarity from large volumes of water.⁴⁹

The water was filtered using pre-combusted GF/F filters (0.2 μm Whatman). Samples were then acidified using HCl (32%) to around pH 2. 10 L of seawater passed through one gram of sorbent, so one cartridge was used for each sample. Pre-extraction, cartridges were rinsed with one cartridge volume of methanol. They were then attached to Teflon tubing and placed in each sample bottle. The sample was passed through the columns using a peristaltic pump. Before elution, salts were removed with 2 cartridge volumes of 0.01 M HCl, and the columns were then dried with air for 5 min. Dissolved organic matter was eluted into glass vials with one cartridge volume of methanol. These 6 mL of eluate were then divided into 1.5 mL glass vials with caps and stored at -20°C until further analysis.

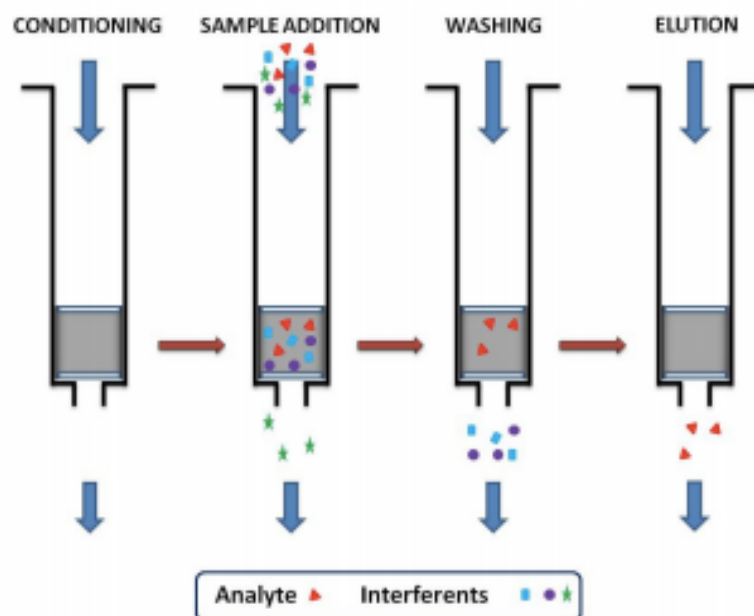


Figure 10. Overview of the SPE procedure. Reproduced from Lucci et al., licensee InTech 2012.

3.6 UPLC-MSE Method

Samples collected the first day containing only Chelex-100 treated seawater along with highest concentrations of DFB and enterobactin were used to develop the LC-MS method.

Non-targeted LC-MS analyses were done on a Waters™ Acquity uHPLC Synapt-G2S Q-TOF system using electrospray ionization (ESI) in positive mode. A Waters™ HSS T3 100 mm column was used for separation with two mobile phases, A: Water (w/ 0.1 % formic acid) and B: Acetonitrile (w/ 0.1 % formic acid). The ESI source used a capillary voltage of 3kV. Leucine enkephalin (1ng/ml with a flow of 10 µl per min) was use as lock mass correction. The injection volume was 4 µL. With a run time of 13.50 minutes, the LC gradient was initially at 94% A and 6% B, after 9 min at 60% A and 40% B, after 12 min at 0% A and 100% B, and finally, after 13 min at 94% A and 6% B. The flow rate throughout was 0.300 ml/min. MassLynx v4.1 SCN871 was used for instrument handling and Progenesis QI V2.2 for data processing. The method was the same for both DFB and enterobactin samples.

4 Data Analysis using Progenesis QI

4.1 Chromatogram Alignment

Once all raw data is imported into the program, the chromatograms are aligned to correct for drifts in retention time. Each sample, or run, is compared to every other and the one with greatest similarity is taken as the alignment reference. Quality control runs contain a small amount of each sample and are run throughout the HPLC-MS method to make sure the conditions remain the same and to prevent errors due to instrument fluctuations. These were selected as reference runs.

The quality of the alignment can then be reviewed. Each run is scored. Low scores indicate poor alignment. When a run is selected, it is shown overlapped with the reference run. Then, specific areas of retention time and m/z are shown highlighted based on alignment quality. Green areas match up exactly, yellow areas are ok, and red areas need review. Using an ion intensity map, manual vectors can be inserted to improve alignment; however, each vector affects the whole m/z range and could result in further poor alignment.

4.2 Experimental Design

Progenesis performs analysis of variance (ANOVA) tests, which are a collection of statistical models to analyze variation, to determine significant differences between ion abundances in samples. In the experimental design section, the user can choose between between-subject or within-subject design.

Within-subject design assumes that each subject is found in more than condition. For example, in experiments performed over time, a sample is taken from one subject at several different times. Conditions are assumed to be related, not independent. Repeated-measures ANOVA is then used to eliminate differences between subjects as a source of variation between conditions. It is an extension of the dependent t-test, which compares the means of two related groups by linking them to an expected difference to see if there is significant variation between them.

In the between-subject experimental design, samples are grouped into conditions, which are assumed to be independent from each other. Since the conditions are independent, if the means are equal across conditions, no variation exists. This represents the null hypothesis.

For this project, compound ions were found based on a between subject design. Conditions were set according to concentration of siderophore. For DFB, 10 nM, 500 nM, and 10000 nM along with a 500 nM no algae control were used. Two more conditions included filtered seawater and 10000 nM no algae samples taken from day 1 of the experiment for comparison. The 10000 nM DFB no algae samples, however, had to be diluted 1 to 50 to avoid overloading the column. For enterobactin, 0.01 nM, 0.5 nM, and 50 nM along with a 0.5 nM no algae control were used. Two more conditions included filtered seawater and 50 nM no algae samples taken from day 1 of the experiment for comparison

4.3 Peak Picking

Peak picking narrows down the parameters from which peaks, and thus compound ions, are selected. For example, you can change the window of retention time to exclude the very beginning, which could be leftovers from the sample before, and the end, which contains all compounds being flushed out of the column. The retention time window chosen excluded the first and last minute for every sample run. Choosing peaks that are above a certain percentage of the base peak eliminates the incorporation of noise. Peaks were chosen greater than 5% of the base peak.

In order to maximize the chance of finding peaks that represent variation between conditions rather than within conditions, the Progenesis user guide recommends not selecting all runs from each condition.⁵⁰ In this project, the first subsample for each bottle was selected for peak picking.

Peaks are then normalized. The default method of normalizing to all compounds was used. In this method, the least different run compared to all others is selected as the reference. The assumption is that many compound ions will not change throughout the samples and will have an abundance ratio of 1. Log abundance ratios of compound ions are then used to find a scaling factor. The median and the absolute median deviation are used to represent the mean and the variance in ratio distribution. The anti-log of the mean of the log(ratios) is then used as the scaling factor.

4.4 Deconvolution

When ESI is used to produce ions, adducts are formed from parent compounds and other elements or molecules surrounding the compounds during ionization such as the solvents used in liquid chromatography. ESI in positive mode produces cations, for example

$[M+H]^+$ or $[M+Na]^+$ where M represents the parent compound. Therefore, two compound ions could be two adducts representing the same parent compound.

In deconvolution, all ions are analyzed and grouped into compounds based on this reasoning. If the difference between the compound ions equals the difference between adduct masses, these two compound ions are grouped to represent the same compound. For example, if the difference in mass between the compound ions $[M+H]^+$ and $[M+Na]^+$ equals the difference in mass between the elements H and Na, these two compound ions represent the same compound.⁵⁰

4.5 Compound Identification

The identify compounds section allows the user to see each compound detected as described by its retention time and m/z. P-values and q-values show how statistically significant each compound is in the variation between conditions. P-values are a result of ANOVA tests that take into account sample size, variance, and mean difference. There will always be abundance differences between experimental groups, but only by taking into account the variation can the statistical significance be determined. The p-value for a compound measures the likelihood of this compound data if no real difference existed. Therefore, the lower the value, the more likely a significant difference does exist. Looking at it another way, a p-value of 0.05 indicates there is a 5% chance for a false positive.⁵⁰

Q-values are obtained from p-values and reduce the problem of multiple testing in which a small percent of false positive quickly multiplies into a large percent. They represent a False Discovery Rate approach that adjusts p-values for each test, lowering the amount of false positives.⁵⁰

Aside from giving each compound a measure of statistical significance, the identify compounds section allows the user to import potential identifications from databases. The three databases used in this project were ChempSpider, Progenesis Metascope, and Metlin. Fragmentation data is also shown when available for each of the compound ions. To match compound ions to database-suggested compounds, a score is given to each of the potential identifications based on isotope distribution, theoretical fragmentation, and m/z.

4.6 Compound Statistics

Principal component analysis, PCA, is then performed using the compound abundances from all runs. This is the statistical method of choice to find interesting patterns

in data sets and to visualize high dimensional space, a result of many variables. To project onto a lower dimensional space, latent variables are produced from a linear combination of the original variables. A new coordinate system is then established, compressing the original data. This system is based on principal components, which describe variation in the data set. The first principal component describes the most variation in the set, and thus the axis for the first principal component goes in the direction of most variation in the original data set.⁵¹

Scores are the new coordinates for an object in the new axes. Scores plots can be used to detect clusters of objects and outliers. Loadings describe how much an original variable contributes to the latent variable. A large loading value for principal component one means this variable contributes strongly to this principal component. Loadings plots can be used to detect clusters of correlated and negatively correlated variables as well as which variables contribute to each principal component. Correlation can be measured by drawing angles from the origin to each variable. If two variables are close to 180° from each other, they are negatively correlated. Close to 0° signifies positively correlation. Close to 90° means there is no correlation.⁵¹ Examples of correlations are graphically represented in Figure 11.

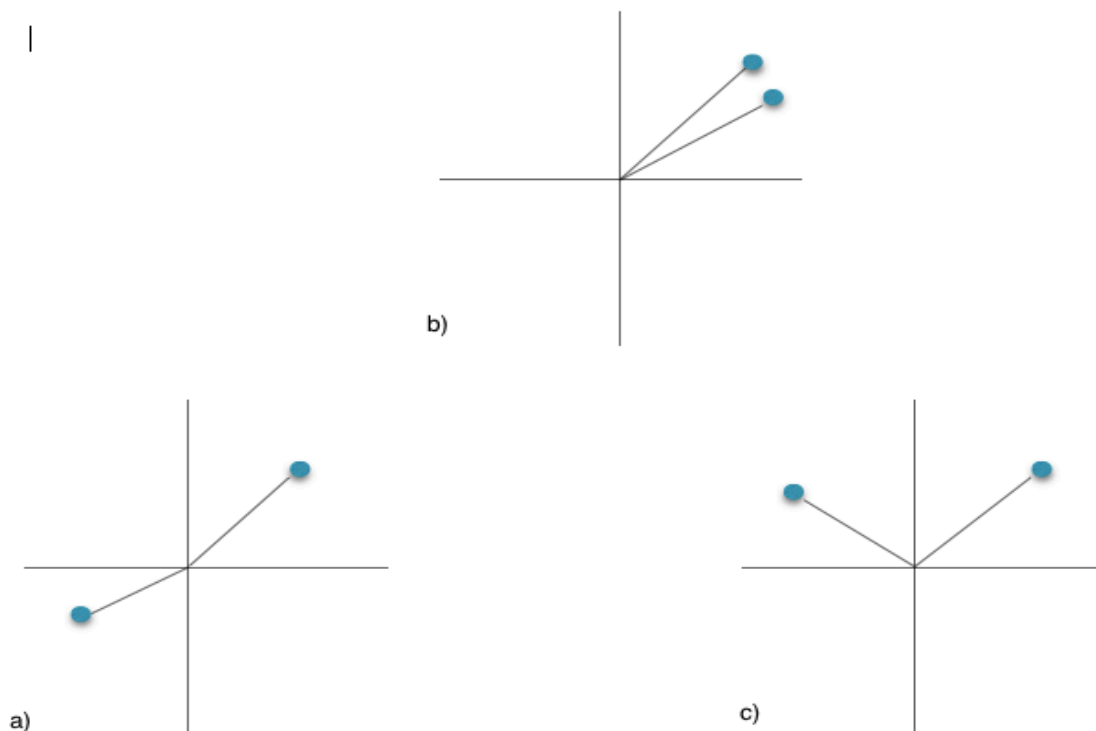


Figure 11. Example loadings plots with variables (represented by dots) negatively correlated (a), positively correlated (b), and not correlated (c)

In the case of this project, the compound ions represent the variables, and the samples, or runs, represent the objects. Progenesis directly provides a PCA biplot, which combines the scores and loadings plots for two principal components. Samples and compound ions are related on a biplot. Drawing a straight line from a compound through the origin to the other side shows which samples this compound influence most. Samples on the positive side of the line have high abundance values for the compound while those on the negative side have low abundance values. The closer a sample is to the axis, the more influence the compound has for that run position.⁵⁰

5 Results and Discussion

5.1 Algal growth

Algal growth could be visually detected after 5 days in the controls containing no siderophores, bottles with the lowest DFB concentration, and all bottles with enterobactin. Significant growth occurred first in the bottles with lower culture volume.

Growth in algae starts with a lag phase followed by an exponential growth phase and then a stationary phase before death.

According to fluorescence data, different trends were seen with the DFB series compared to enterobactin. As shown in Figure 12, signs of exponential growth, indicated by an increase in fluorescence, were seen first in bottles containing the lowest concentrations, 10 nM and 50 nM, of DFB around day 5. The 500 nM set then began to show signs followed by the 2500 nM and the 10000 nM sets. The control in this data contained algae with no siderophore added.

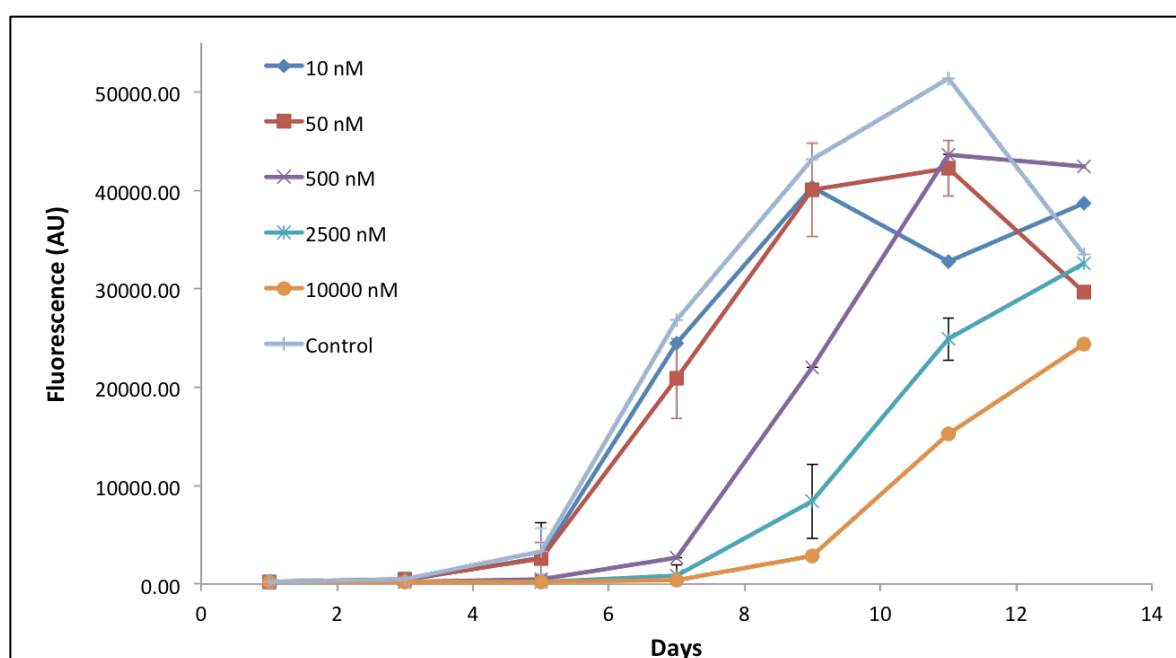


Figure 12. *in vivo* fluorescence, 441/82 nm excitation, of DFB samples.

In previous experiments at NTNU examining the effect of siderophore concentrations on diatom growth under controlled iron concentration conditions, diatoms showed no signs of growth at first but eventually began to grow in the presence of large amounts of siderophores.

In literature, some studies show increased growth of diatoms in the presence of DFB³² while others show decreased growth of diatoms in the presence of DFB³³. This experiment shows an initial suppression of growth followed by growth, with the length of suppression influenced by concentration. Samples with the largest siderophore concentration of 10000 nM, which was expected to substantially decrease iron bioavailability, showed no signs of algal growth until day 9, when exponential growth began to be seen. Using this as a guideline, the large bottles were sampled for organic matter analysis for the DFB series on day 9. This day represents a time when the algae in all samples besides the control had exponential phase growth.

The same trend was not clearly seen in the enterobactin samples (Figure 13). The first signs of fluorescence came for all samples on day 5 and continued with the same trends. The standard deviation shows overlap in the measurements for all bottles in day 5 and 7, and in all bottles except for those with 0.01 nM on day 9. The growth in these bottles plateaued around day 9. In contrast to the DFB samples, these showed higher fluorescence in the lower concentrations compared to the control. Due to the inability to carry all sample bottles back to the lab for analysis, these were sampled after DFB on the final day of the experiment.

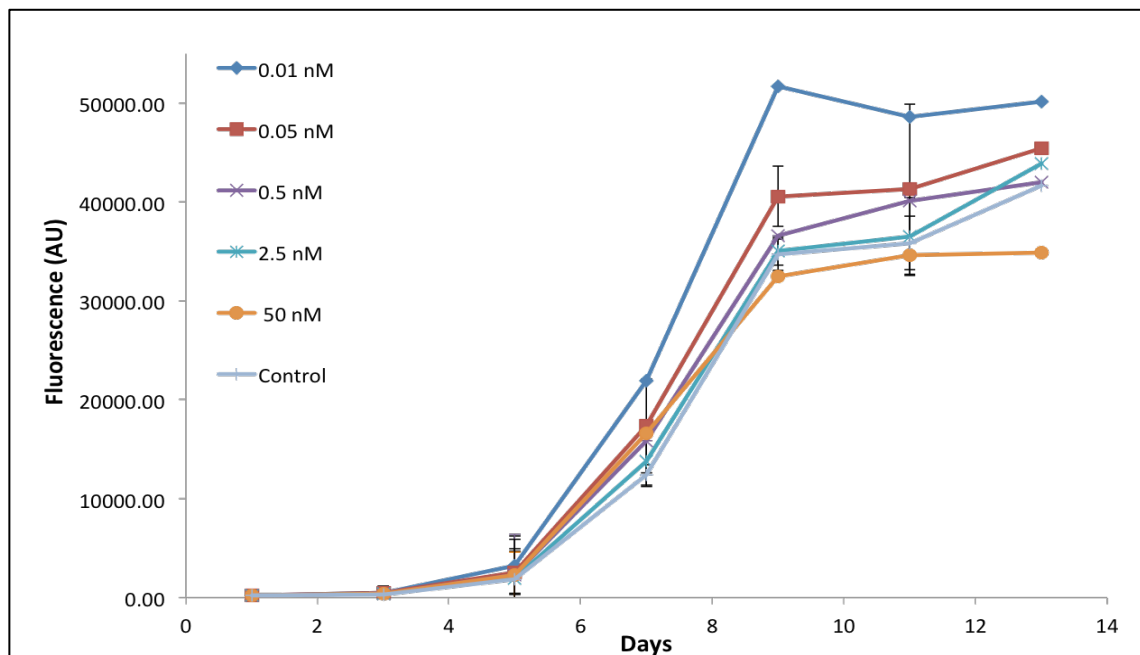


Figure 13. *in vivo* fluorescence, 441/82 nm excitation, of enterobactin samples

A study by Strzepak et al., which examined the effect of low iron conditions and siderophores on Southern Ocean diatom growth rate, found that some species which could grow in the presence of DFB bound iron could not grow with enterobactin present.³⁴ Other species in the same study that did grow in the presence of enterobactin required greater than

10 fold excess concentration of siderophore to limit growth.³⁴ This could be a sign that the low concentrations of enterobactin used were not large enough to show the same clear trend as with DFB. The three lowest concentrations were under the concentration of Chelex-100 labile iron measured to be 1.2 ± 0.5 nM. However, the largest concentration at 50 nM should have shown an effect on growth. The diatom was able to reduce a sufficient amount of iron to maintain growth under the enterobactin conditions.

The study used enterobactin and DFB pre-complexed to Fe before use in the diatom growth media. In this experiment, enterobactin was added without pre-complexation. An inability of this siderophore to complex iron in the media could also explain the growth of the diatom in the enterobactin series.

5.2 DFB Series

5.2.1 Compound Ions Discovered

From the LC-MS data, 78 compound ions were discovered. These showed significant differences in abundance between conditions as demonstrated by p-values < 0.05 for each compound. 54 of these were then identified using a combination of three databases available in Progenesis: Metlin, Progenesis Metascope, and Chempid. Compound ions further discussed in the next sections are shown in Table 1.

Compound ion (m/z)	Retention time (min)	Suspected Origin	Potential Siderophore Metabolite	Matches metabolite chemical formula	Database Identification
201.1240	4.31	Siderophore	Yes	Yes	Pantothenamide
319.2335	2.87	Siderophore	Yes	No	Istamycin
319.2348	4.26	Siderophore	Yes	No	Istamycin
361.2715	3.18	Siderophore	Yes	No	Glycidyl oleate
419.2503	3.41	Siderophore	Yes	Yes	Thr Leu Val Ser
561.3616	4.30	Siderophore	-	-	DFB
571.1693	5.09	Algae	-	-	Glucoronide
614.2710	2.95	Siderophore	-	-	Ferrioxamine

Table 1. Potential chelators discovered in the DFB series.

5.2.2 Identifying DFB and Ferrioxamine

During alignment, it was seen that the highest siderophore concentration of experimental samples had alignment issues around the expected retention time and mass to

charge ratio (m/z) of DFB, 4-5 minutes and 561 m/z (Figure A.1). This could be a result of overloading as shown by the broad tailing peak at 4.17 min in the chromatogram for a sample from a 10000 nM experimental bottle (Figure 14). Since the alignment problems only affected this small region of retention time and m/z , no further steps were taken to correct the issue. Attempts at manual alignment caused additional problems elsewhere in the spectrum.

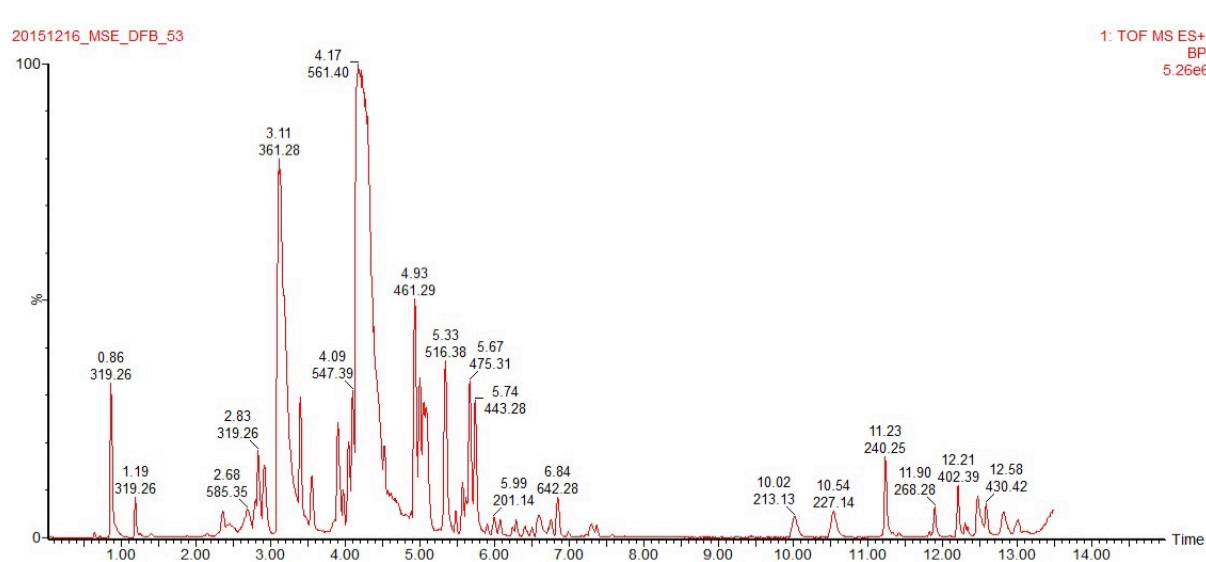


Figure 14. Mass spectrum of a 10000 nM DFB experimental sample.

This could result in altered abundances for molecules such as DFB in the affected region. If some samples have the DFB peak at slightly different retention times than others, comparison of the compound between samples is affected. This also decreases the reproducibility of the results.

Despite these alignment issues, the siderophore, DFB, and its complex with iron, ferrioxamine, were found among the compound ions. The column in the LC system used retains nonpolar, hydrophobic compounds more strongly, and the more hydrophilic ferrioxamine molecule eluted before DFB. DFB was identified at a retention time of 4.30 minutes and with an m/z value of 561.3616. The fragmentation spectrum matched that found in literature with high intensity fragments at 201 and 243 m/z (Figure 15).²⁸ Ferrioxamine was found at 2.95 minutes and 614.2710 m/z . No fragmentation data was obtained for this compound, but the presence of iron was confirmed using the ^{54}Fe , ^{56}Fe isotopic ratio (Figure 16), with ^{54}Fe about 6% of ^{56}Fe . This pattern of peaks surrounding 614 match those used in previous research using mass spectroscopy to characterize iron-bound siderophores.²⁸

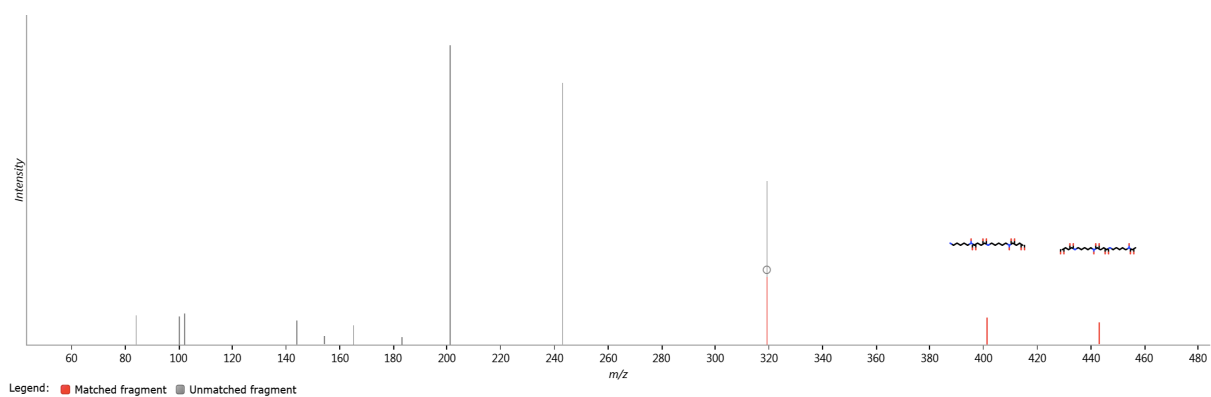


Figure 15. Fragmentation spectrum for DFB

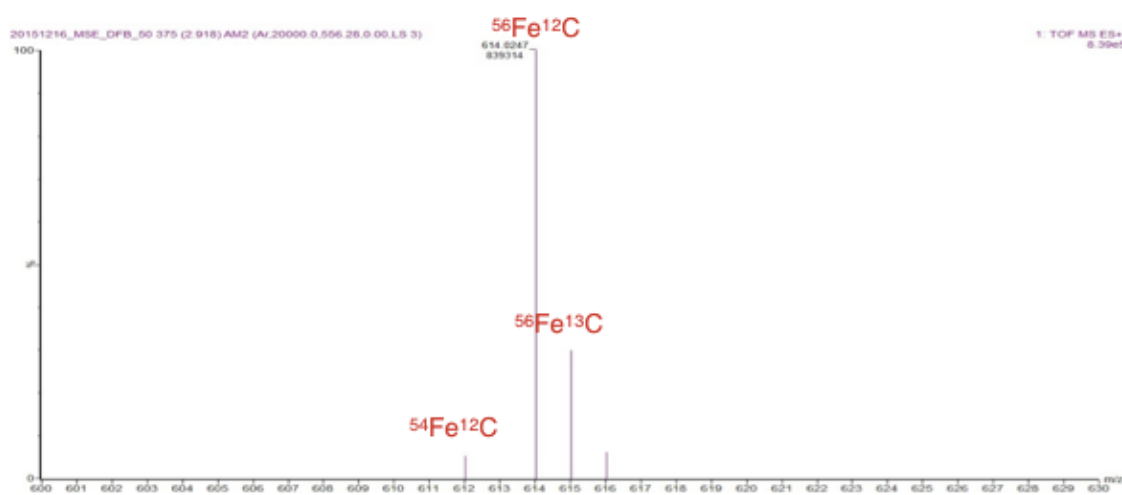


Figure 16. Mass spectrum highlighting ferrioxamine at 614 m/z and its iron isotopic pattern



Figure 18. Abundance profile for DFB. From left to right: 10 nM, 500 nM, 10000 nM, noAlgae 500 nM, colors correspond to those on the PCA.



Figure 19. Abundance profile for ferrioxamine. From left to right: 10 nM, 500 nM, 10000 nM, noAlgae 500 nM, colors correspond to those on the PCA.

Figures 18 and 19 show the standard normalized abundance profiles for DFB and ferrioxamine in all samples. In the PCA biplot, sample runs are shown as colored dots and compound ions as grey numbers (highlighted compounds show up as red). Based on the PCA biplot (Figure 17), samples were appropriately grouped into conditions: samples taken from different experimental siderophore concentrations were significantly different from each other, while those from the same experimental condition were similar. This is shown by runs in each condition forming clusters and no overlapping occurring between clusters. The color-coded conditions match those shown in the abundance profiles, with blue dots representing the 10 nM DFB samples, purple dots representing the 500 nM DFB samples, yellow dots representing the 10000 nM DFB samples, and green dots representing the 500 nM DFB, no algae samples.

The first principal component accounted for about 60% of the sample variance and separated the highest DFB concentration and control from both of the lower DFB

concentrations. Considering the 10000 nM samples just began to show exponential growth and the control contained siderophore with no algae, it can be hypothesized that this component relates to the existence of algae in the samples. It is also possible this is related to the presence of DFB, since that has highest abundance in the 10000 nM and 500 nM no algae. The second component, describing about 25% of the variance, separated the 10 nM DFB samples from the 500 nM DFB samples but had little effect on the 10000 nM DFB samples and the no algae control. The third principal component, accounting for only 6% variance, separated the 10000 nM samples from the no algae control (Figure A.2).

The scores plot (Figure A.3) further confirms the grouping into conditions. Runs from the same condition are clustered together. The 10000 nM and 500 nM no algae conditions are grouped closely together and have little effect on the second principal component. However, the 500 nM and 10 nM samples are separated by the second principal component.

The abundance of DFB, identified by its retention time and m/z in the PCA, is positively correlated to the 10000 nM DFB samples and the no algae 500 nM DFB control and negatively correlated to the lower DFB concentration samples. According to the loading values, it contributes more to the first and third principal components than the second (Figures A.4 & A.5).

Ferrioxamine shows the opposite trend with abundance positively correlated with the lower concentration samples and negatively correlated with the control and highest concentration samples. Based on the loadings data, it equally contributes to components one and two and less to component three (Figures A.4 & A.5).

The abundance of DFB and ferrioxamine are negatively correlated according to the loadings and biplot data (Figure A.4). If it is assumed the amount of background iron is constant, the amount of iron-bound siderophore, ferrioxamine, should be fairly constant throughout the samples. Introducing algae, which also take up available iron, it could be expected that the samples with more algal growth, the lower concentration samples, would show the least ferrioxamine. Over time, the algae are able to uptake iron from the organic ligands. This is not shown in the results, with the higher siderophore concentration samples and even the no algae control showing less abundance of ferrioxamine than the lower concentration siderophore samples.

Other compounds eluting at the same time could block the signal for ferrioxamine. A cholesterol compound was identified at the same retention time. However, it would be expected that more algal content would lead to a greater likelihood for iron suppressing compounds. There are also many sources of iron contamination in the LC/MS system,

affecting the amount of ferrioxamine and DFB. It is likely the samples had higher concentrations of iron due to the column and tubing. Some samples could have been more contaminated than others.

It should be noted that the abundance of a compound ion cannot be directly related to concentration since in this qualitative method, signals for compounds do not necessarily behave the same in the mass spectrometry system. In other words, different compounds can show different abundances even though they have the same concentration in the sample. The same compound can also behave differently each time it is ionized and detected depending on the surrounding molecules. A different MS system is needed and a linear curve based on standards of known concentrations must be established for each compound before acquiring concentrations for unknown standards. However, trends over conditions for a single compound can be seen using the abundance. A clearer trend is seen in the DFB abundance data (Figure 18), where the 10 nM and 500 nM samples have lower abundances than the 10000 nM and 500 nM no algae samples, than the ferrioxamine abundance data (Figure 19), which shows a high abundance in only some of the 500 nM samples.

5.2.4 Potential DFB Metabolites

The search for potential DFB metabolites was based on previous research by Winkelmann et al.⁵² and Pierwola et al.⁵³ on the degradation of DFB by the bacteria *Azospirillum irakense* and detection of metabolites using ESI-MS. In these studies, the bacteria degraded the un-complexed siderophore into a sequence of dihydroxamates and monohydroxamates. From the molecules outlined in Figure 20, the two dihydroxamates found at 361 m/z and 419 m/z along with the monohydroxamate found at 319 m/z matched mass to charge ratios of compound ions discovered in this method.

Desferrioxamine B *m/z* 561

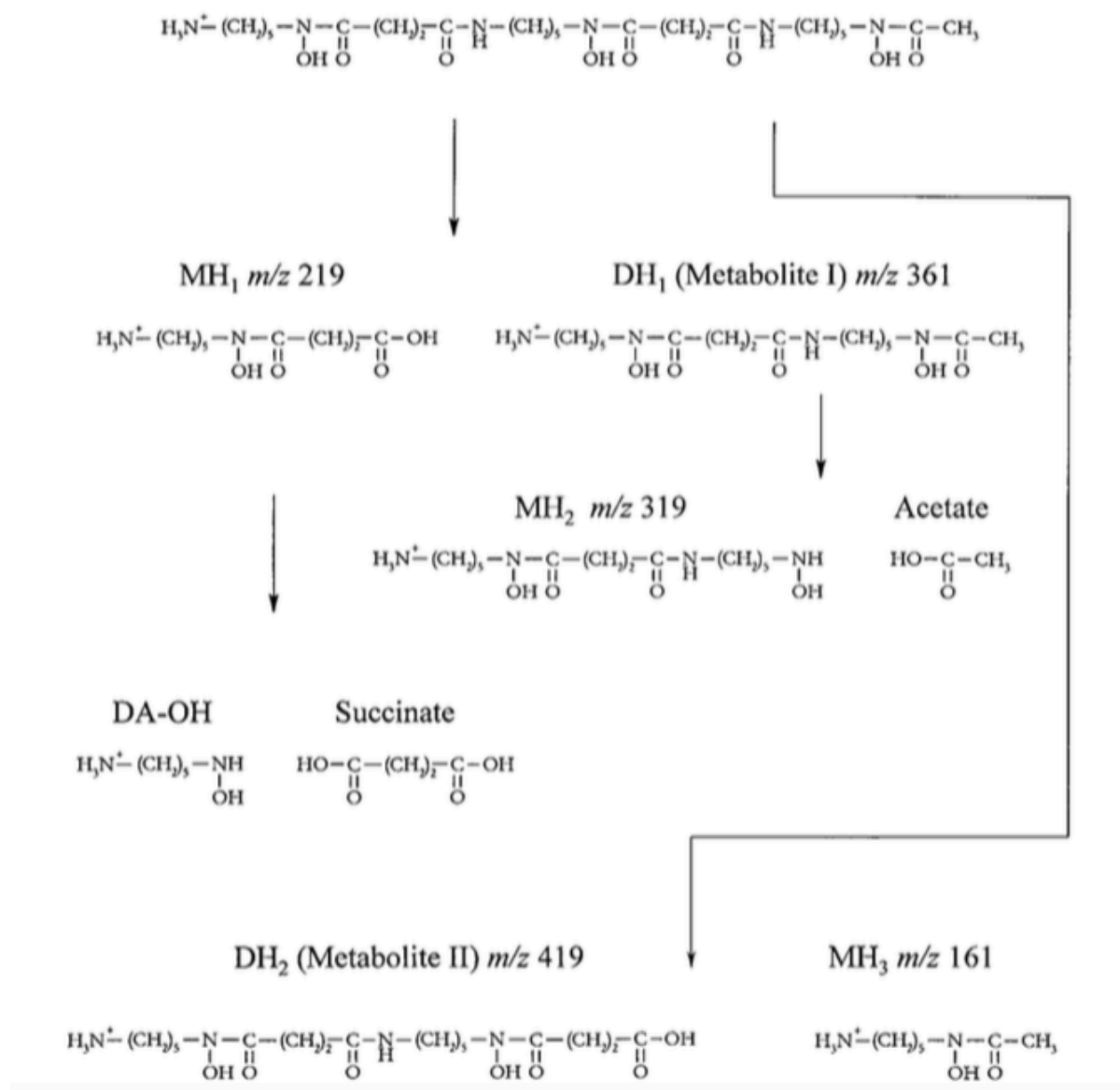


Figure 20. Degradation of DFB by the bacteria *Azospirillum irakense*. Reproduced from Winkelmann et al.⁵²

A potential dihydroxamate compound ion with 361.2715 *m/z* eluted at 3.18 minutes and was found to be in a cluster of compounds close to DFB on the PCA, indicating a positive correlation (Figure A.6). However, the suggested chemical formula did not include any nitrogens, indicating it probably was not a metabolite of DFB, and the databases identified it as a glycidyl oleate, which is a fatty acid derivative.

Another potential dihydroxamate compound ion with 419.2503 *m/z* eluted at 3.41 minutes and matched the chemical formula for the second dihydroxamate shown in Figure

20. According to the PCA, it was most abundant in the 500 nM samples (Figure A.7). However, the loadings data indicates there is no correlation between this compound and DFB (Figure A.14), and structural information for suggested compounds did not exactly match.

Potential compound ions of the monohydroxamate 319 m/z were found. One with 319.2335 m/z eluted at 2.87 minutes and another with 319.2348 m/z eluted at 4.26 minutes. Both were found close to DFB in the PCA (Figures A.8 & A.9). However, the databases suggested a different chemical formula from the monohydroxamate, and both these compounds were identified as istamycin, which is an aminoglycoside antibiotic. Marine bacteria have been found to produce more istamycins when polysaccharides are used as carbon sources than when mono or disaccharides are used.⁵⁴ Both show highest abundance in the 10000 nM samples (Figures A.8 & A.9), which could suggest the diatoms are releasing large amounts of polysaccharides to chelate iron during the start of their growth under high siderophore concentration conditions.

Previous research on fragments of DFB discovered using collision induced tandem mass spectroscopy was also looked into.⁵⁵ In this MS technique, ions are accelerated so that they collide with one another, breaking bonds and giving information into a molecule's structure based on its fragments. Figure 21 shows how the major fragments, 201 m/z and 243 m/z, are formed.

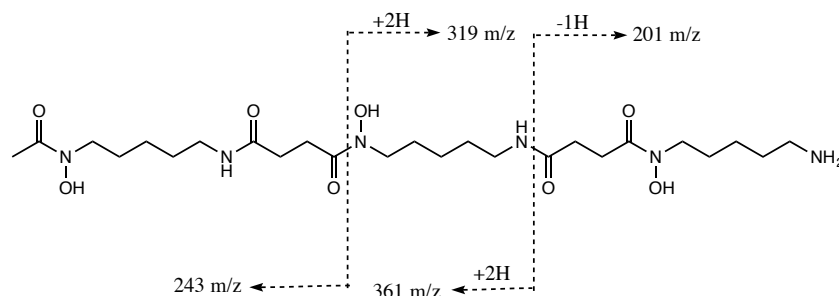


Figure 21. DFB fragmentation from collision induced tandem MS (adapted from Groenewold et al.).⁵⁵

319.257, 201.1379, and 243.1512 m/z were found eluting at the same time as DFB, 4.30 minutes, and clustered with it in the PCA. However, structural information from the databases and chemical formulas did not match those shown in the figure.

At 4.31 minutes, 201.1240 and 243.1341 m/z compound ions also eluted. The first had the same suggested chemical formula as shown in Figure 21 and had the highest abundance in the 500 nM samples (Figure A.10). As shown in the PCA and loadings data, it is not strongly correlated to the DFB compound ion (Figure A.14). The suggested compound

was a pantothenamide, which inhibits bacterial growth.⁵⁶ The second matched the 243 m/z fragment in regards to chemical formula, but showed a high abundance in the seawater blanks (Figure A.12), indicating it was not a DFB derivative.

Overall, no metabolites were conclusively found based on the database suggestions. However, the two most promising, the 419 m/z dihydroxamate and the 201 m/z fragment, were both found to have the highest abundance in the 500 nM samples. If degradation of the siderophore was to occur, it could be expected that the most metabolites would be seen not just in the 500 nM samples, but in all samples with a lot of algae growth and in the 10000 nM samples, when the algae had just begun to grow. This would indicate that the siderophore-iron complex was being broken down, or the DFB molecule itself had released its iron and was prevented from complexing further, allowing iron to become bioavailable and more algae to grow. However, considering the 500 nM samples were “mid-way” between the 10 nM and 10000 nM samples in their exponential growth phase, it is possible these had the most metabolites since the samples with less growth had fewer degraded DFB and the samples with the most growth had either further broken down metabolites or a greater amount of organic material with the potential for ion suppression.

5.2.5 Non-DFB Related compounds

Along with the istamycin found in the search for DFB metabolites, another aminoglycoside antibiotic, gentamicin, was discovered also positively correlated to DFB in the PCA. A range of other compounds was identified by the databases as molecules from anti-histamines, anti-depressants, or heart and circulation drugs.

Compounds produced by phytoplankton to bind iron include saccharides such as glucuronic, glucaric, or uronic acids.^{23, 57} Glucuronide is a derivative of glucuronic acid and was identified eluting at 5.09 minutes and with 571.1693 m/z. According to the PCA, this had most positive abundance in the 10 nM and 500 nM samples, which is where the most algal growth was seen (Figure A.13). This could be a sign that molecules excreted by algae can outcompete DFB for iron, leading to algal growth.

5.3 Enterobactin Series

5.3.1 Compound Ions Discovered

89 compound ions were found using Progenesis. 67 of these were identified using a combination of three databases available: Metlin, Progenesis Metascope, and Chemspider. 58 of the 89 showed significant differences in abundance between conditions as demonstrated by low p-values for each compound. Compounds discussed in the next sections are shown in Table 2.

Compound ion (m/z)	Retention time (min)	Suspected Origin	Database Identification
516.2552	10.81	Algae	Eriojaposide B
541.2616	9.35	Algae	Blumenol glucoside
670.1525	9.81	Siderophore	Enterobactin
695.2918	6.79	Algae	Nomilinic acid glucoside

Table 2. Potential chelators discovered in the enterobactin series.

5.3.2 Identifying Enterobactin

The siderophore was found eluting at 9.81 minutes, towards the end of the time window, indicating the hydrophobic nature of the molecule. It had 670.1525 m/z (Figure 22). The compound's identity was further confirmed by its fragmentation data, with the primary fragment 224 m/z being one third of the original molecule (Figure 23). No fragment indicating two thirds of the molecule at 447 m/z was seen. Enterobactin complexed with iron was not found.

In animals, enterobactin's hydrophobicity results in it being an ineffective iron scavenger for the bacteria that produce it due to it partitioning in lipid bilayers in mammalian cells. Modifications through glycosylation makes it less hydrophobic and increases its iron-scavenging ability.⁵⁸ In marine systems, unmodified enterobactin would also partition into the lipid bilayers of diatom cells, affecting its ability to keep complexed iron in solution and leading to no iron complex found in the MS data. Despite enterobactin being a powerful ferric iron complexing agent, its hydrophobicity prevented it from significantly affecting iron bioavailability and diatom growth at the highest concentration used.

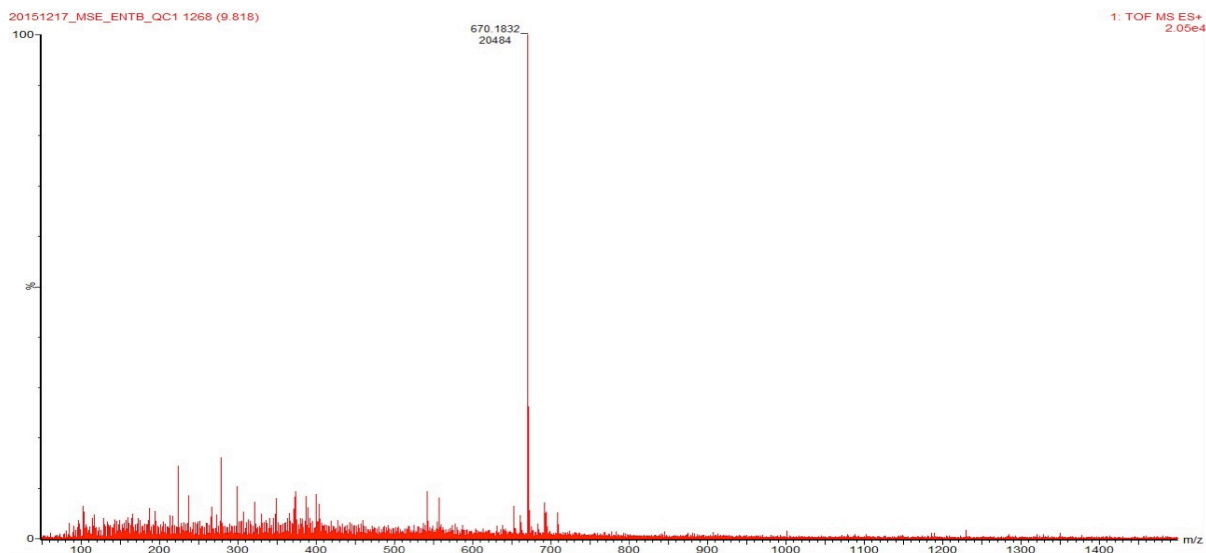


Figure 22. Enterobactin peak at 670 m/z.

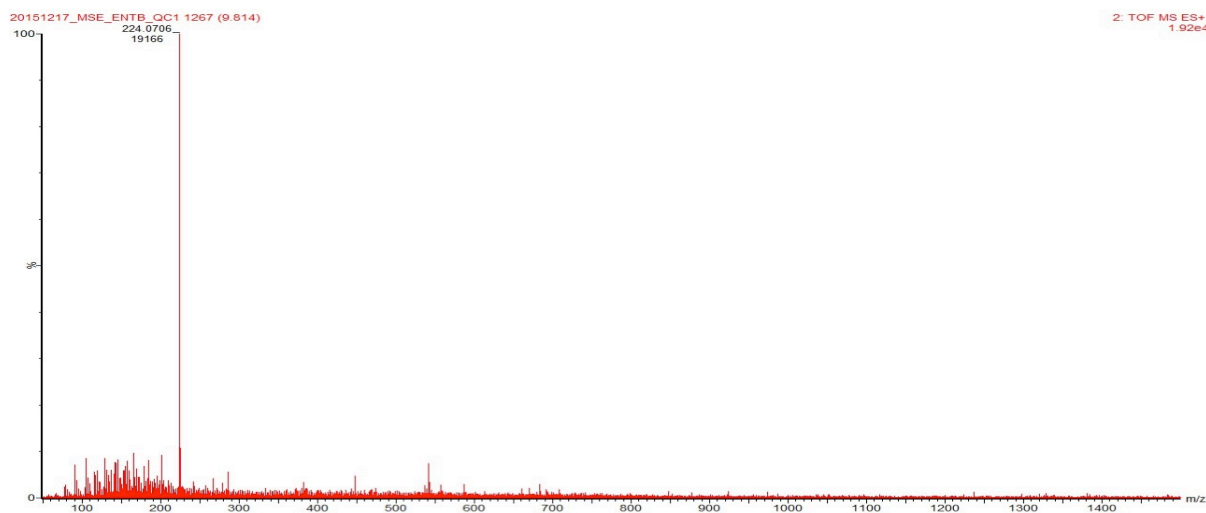


Figure 23. Fragmentation of the identified enterobactin compound, with 1/3 of enterobactin at 224 m/z.



Figure 25. Enterobactin Abundance Profile. From left to right: 0.01 nM, 0.5 nM, 50 nM, noAlgae 0.5 nM, colors correspond to those on the PCA.

Figure 25 shows the abundance profile for enterobactin in all samples. In the PCA biplot, sample runs are shown as colored dots and compound ions as grey numbers (highlighted compounds show up as red). The color-coded conditions match those shown in the abundance profile, with blue dots representing the 0.01 nM enterobactin samples, purple dots representing the 0.5 nM enterobactin samples, yellow dots representing the 50 nM enterobactin samples, and green dots representing the 0.5 nM enterobactin, no algae samples.

Based on the PCA biplot (Figure 24), samples did not cluster based on condition. The no algae 0.5 nM samples showed the most similarity but were still spread out, particularly along the second principal component. Each sample bottle had three subsamples that were analyzed by MS, and these represent the clusters shown on the PCA for the algae containing samples. The scores plot (Figure A.15) also shows overlap of conditions, indicating conditions were not significantly different from each other.

The first principal component separates the algae from the non-algae samples and accounts for 56% of the variance. The second principal component, accounting for 22% of the variance, seems to separate the two sample bottles for the 0.01 nM and 0.5 nM samples.

The abundance profile shows no clear trend across conditions for enterobactin, although the compound ion was found to be significant between conditions with a low p-value.

5.3.4 Non-Enterobactin Related Compounds

From the many compounds identified, two glucosides and a glycoside were discovered which originated from the algae present in the system. These included nomilinic acid glucoside found at 6.79 minutes and 695.2918 m/z; eriojaposide B found at 10.81 minutes and 516.2552 m/z; and blumenol glucoside found at 9.35 minutes and 541.2616 m/z.

As seen from the PCAs, eriojaposide B and blumenol glucoside are more positively correlated with the highest enterobactin concentration samples while nomilinic acid glucoside is more positively correlated with the lowest concentration samples (Figures A.17, A.18, and A.19). According to the loadings data, eriojaposide B and blumenol glucoside are positively correlated with enterobactin while nomilinic acid glucoside has no correlation (Figure A.16). Nomilinic acid glucoside was the only one of these compounds with a p value < 0.05, indicating it showed significant differences between conditions.

According to the Human Metabolome Database, all of these compounds are associated with the leaves of fruit trees. All are classified in the group lipids and saccharides, but eriojaposide B and blumenol glucoside are more closely related as disaccharides with similar structures.⁵⁹ These two are also more hydrophobic as shown by their high retention times.

5.4 Comparing DFB and Enterobactin

The algal cultures containing enterobactin showed less limitation of algal growth and on some days an increase in growth compared to the control. This could be a result of the low concentrations used, some of which were below the 1.2 ± 0.5 nM measured for Chelex-100 labile iron in the samples, and the ability of the diatoms to uptake the iron bound to the siderophores. The hydrophobicity of the siderophore also inhibited its ability to complex iron and stay dissolved in the water, instead retreating to the lipid bilayers of the diatom cells. Using MS to analyze enterobactin is hindered by the fact that the molecule degrades easily due to its ester linkages.³⁸ Binding Fe(III) is also pH dependent. At pH values below 4, uncoordinated sites exist in the iron-siderophore complex, or there is complete dissociation.⁶⁰ Since the SPE method used included an acidifying step, it is possible any iron bound enterobactin molecules were degraded, affecting their discovery in the MS data. At low pH, it has been shown that Fe(III) associates with only two of the three serine groups, forming a singly charged anion that has been detected by ESI in negative mode, rather than the positive mode used.³⁸ This acidification could also lead to dissociation of iron from some of the ferrioxamine compounds in the DFB series.

Due to the increased algae content in the enterobactin samples and a limited supply of filters, more organic matter likely passed into these samples than the DFB samples. This created an environment with more compound ions, which could also have masked the signal for the iron bound enterobactin or any enterobactin metabolites.

Since there was a small amount of enterobactin compared to other organic compounds, the conditions based on siderophore concentration no longer separated the samples in the PCA. Some of the identified compounds did not significantly change between conditions, and samples within the same condition showed differences in the compounds they contained. No potential enterobactin metabolites or iron bound molecules were discovered and similar algal growth in all samples led to difficulty in drawing comparisons between compounds. No clear signs that the amount of siderophore influenced the type of compounds present in the system were discovered. Although the compound ion was found to vary significantly between conditions based on its low p-value, the abundance profile for enterobactin shows no clear trend throughout the samples.

Conversely, high concentrations of DFB clearly limited the bioavailability of iron to the diatoms initially, and the samples containing lower concentrations of siderophore exhibited algal growth before those with higher concentrations. The PCA showed a clear separation of samples based on siderophore concentration, indicating the discovered compounds varied between conditions but were consistent within a condition. This allowed for comparative analysis of compounds, which was not achievable in the enterobactin series.

The abundance profile for DFB showed an increase in the 500 nM no algae samples compared to the 500 nM samples with diatom growth. This is a sign that the compound is changing in the presence of algae.

Increased literature on MS analysis of hydroxamate siderophores and DFB in particular allowed a greater number of potential metabolites to be investigated than in the case of enterobactin. The HPLC-MS method, however, lacks sensitivity and reproducibility due to the peak tailing property of DFB as seen in the alignment. This has been documented as a challenge in the HPLC-MS analysis of DFB, particularly in quantification studies.⁶¹

Although ferrioxamine was detected, its abundance did not show a trend throughout samples but rather a spike in some of the 500 nM samples. Also, potential metabolites that matched m/z and chemical formulas of fragmentation or degradation products of DFB could not be confirmed by database suggested structures.

Several factors affected the findings from both sample sets. One was the quality of the DOM extraction process, which affects which compounds and how much of each were collected from the original samples. The enterobactin samples showed differences in compounds found in each sample bottle rather than each condition. Others came from the MS system including iron contamination and the potential that some compound signals were

suppressed due to the untargeted nature of the approach and the amount of organic material present in the samples.

Another factor was the use of methanol as the sample diluent injected into the LC system. Since methanol is less polar than the water mobile phase, once injected, the sample formed a plug that was dissolved over time. This results in compound ions being found in peaks throughout the chromatograms, not just in one peak. For example, the two potential metabolites with 319 m/z identified as istamycin eluted at both 2.87 min and 4.26 min. Slight differences in m/z could have prevented the databases from identifying compounds that were the same: for example, in the DFB series, many unidentified compounds had close to 561.4 m/z, with the identified DFB compound having 561.3616 m/z. Along with compound identification, this affects the abundances for compounds. Preventing this spread of peaks by dissolving the samples in water would increase the reproducibility of the method. The injection volume, however, was very low at 4 μ L, and the qualitative nature of the method only required compound ions to be found and no concentrations to be calculated.

5.5 Future work

This project only gave a snapshot of the organic material present in the samples during diatom growth. Samples were taken for organic analysis only once for each siderophore concentration condition. Widening the sampling to give a time series over the course of the diatom life cycle would allow compounds to be compared from different stages under the same siderophore condition. Comparing specific compounds over the course of the diatom growth period would add another dimension to the results by showing trends in which compounds are present before and after algae begins to grow for each siderophore condition. This could then be compared over different conditions, different concentrations of siderophore.

The experimental setup could also be improved in the future by adding a control containing algae with no siderophore grown under low iron culture conditions. In this project, a siderophore, no algae control was designed to show any natural degradation of the siderophore in the medium. However, also having an only algae control could give a reference for compounds only originating from algae. If samples with algae and added siderophore showed compounds that were not present in the only algae control and the only siderophore control, evidence could be shown that these compounds were a result of the interactions between algae and siderophores.

In order to better identify potential compounds and track them throughout the experiment, a certain number of known compounds could be selected that can then be analyzed on their own, establishing m/z, isotope, and fragmentation data that can be stored in a database. This database can be used in future data analysis to target these molecules in new unknown samples.

Since ferrioxamine and DFB are detected using ESI in (+) mode, only this method was used. However, methods for detecting aliphatic hydroxy carboxylic acids, including the uronic and glucaric acids released by algae to chelate iron, have been established using anion exchange chromatography coupled with MS using ESI in (-) mode.⁶² One method alone may not be ideal to detect all potential iron complexing compounds. Using other methods such as ESI in negative mode could lead to the discovery of more compounds that were not detectable with the method in this project as well as the anionic form of enterobactin with exposed coordination sites.

6 Conclusion

The two siderophores studied showed different effects on the growth of *Skeletonema costatum*. Based on fluorescence data, DFB suppressed growth of the diatom initially before growth was seen sequentially in samples from lowest to highest siderophore concentration. By day 9 all samples showed exponential phase growth of the diatom.

In the presence of enterobactin, all samples began to show signs of fluorescence at the same time on day 5. The different concentrations showed less of a difference in growth for this siderophore, but the lowest concentration samples showed increased fluorescence compared to the others and compared to the control. Although enterobactin is known as a powerful ferric iron complexer, its hydrophobicity affects its ability to scavenge iron in marine systems.

Using ESI-MS, both siderophores along with DFB's iron complex, ferrioxamine, were identified. Possible DFB metabolites that matched m/z and chemical formulas were found, although no structural matches were suggested by the databases used in Progenesis. The siderophore metabolites showed high abundances in the 500 nM DFB samples, which contained diatoms midway through exponential phase growth. Ferrioxamine abundance was also high in 500 nM samples and was generally higher in samples showing more algal growth, which was opposite of the theory that less iron complexed siderophore would be seen when algae were growing, using iron that had previously been complexed.

Compounds produced by the cultured diatom and bacteria were also detected. Saccharides and their derivatives were found which are produced by algae and have the ability to chelate iron. Several antibiotic compounds produced by bacteria were also discovered.

In the DFB series, the discovered compound ions showed significant differences between conditions, confirming the organic matter in each sample varied based on the concentration of siderophore in the sample. Further experiments are needed to understand these differences, taking into account a wider range of samples over time and incorporating a more targeted approach – tracking the added siderophores along with a few known chelating compounds released from algae. This project serves as a useful reference in developing future experiments. The characterization of iron complexes in the marine system using MS is a relatively new field of study with the potential to elucidate the interaction between iron and

chelators, thus uncovering dimensions of the relationship between algae and bacteria in the oceans.

Bibliography

1. Boyd, P.; Ellwood, M., The biogeochemical cycle of iron in the ocean. *Nature Geoscience* **2010**, *3* (10), 675-682.
2. Duce, R. A.; Tindale, N. W., Atmospheric transport of iron and its deposition in the ocean. *Limnology and Oceanography* **1991**, *36* (8), 1715-1726.
3. Prospero, J. M.; Uematsu, M.; Savoie, D. L., Mineral Aerosol Transport to the Pacific Ocean *Chemical oceanography* **1989**, *10*, 187.
4. Arimoto, R.; Duce, R.; Savoie, D.; Prospero, J., Trace elements in aerosol particles from Bermuda and Barbados: Concentrations, sources and relationships to aerosol sulfate. *Journal of Atmospheric Chemistry* **1992**, *14* (1-4), 439-457.
5. Ardelan, M.; Holm-Hansen, O.; Hewes, C.; Reiss, C. S.; Silva, N.; Dulaiova, H.; Steinnes, E.; Sakshaug, E., Natural iron enrichment around the Antarctic Peninsula in the Southern Ocean. *Biogeosciences* **2010**, *7* (1), 11-25.
6. Dulaiova, H.; Ardelan, M.; Henderson, P. B.; Charette, M. A., Shelf - derived iron inputs drive biological productivity in the southern Drake Passage. *Global Biogeochemical Cycles* **2009**, *23* (4).
7. Bruland, K. W.; Rue, E. L., Iron: Analytical methods for the determination of concentrations and speciation. *The Biogeochemistry of Iron in Seawater* **2001**, 255-289.
8. Price, N. M.; Morel, F. M., Biological cycling of iron in the ocean. *Metal ions in biological systems* **1998**, *35*, 1-36.
9. Gledhill, M.; Buck, K. N., The organic complexation of iron in the marine environment: a review. *The microbial ferrous wheel: iron cycling in terrestrial, freshwater, and marine environments* **2012**, 29.
10. Liu, X.; Millero, F. J., The solubility of iron in seawater. *Marine Chemistry* **2002**, *77* (1), 43-54.
11. Shaked, Y.; Lis, H., Disassembling iron availability to phytoplankton. *Environmental Bioinorganic Chemistry of Aquatic Microbial Organisms* **2012**, 28.
12. Kenshi, K., Biogeochemistry of Iron in Seawater. *Report on Amur-Okhotsk Project (2)* **2004**.
13. Stumm, W., and Morgan, James J., *Aquatic Chemistry*. Third Edition ed.; John Wiley & Sons, Inc. : 1996.
14. Sarthou, G.; Bucciarelli, E.; Chever, F.; Hansard, S.; Planchon, J.; Speich, S.; González-Dávila, M.; Santana-Casiano, J. M., Labile Fe (II) concentrations in the Atlantic sector of the Southern Ocean along a transect from the subtropical domain to the Weddell Sea Gyre. **2011**.
15. Martin, J. H., Glacial - interglacial CO₂ change: The iron hypothesis. *Paleoceanography* **1990**, *5* (1), 1-13.
16. Baar, H. d., On iron limitation of the Southern Ocean: experimental observations in the Weddell and Scotia Seas. *Mar. Ecol. Prog. Ser.* **1990**, *65*, 105-122.
17. Boyd, P. W.; Jickells, T.; Law, C.; Blain, S.; Boyle, E.; Buesseler, K.; Coale, K.; Cullen, J.; De Baar, H.; Follows, M., Mesoscale iron enrichment experiments 1993-2005: Synthesis and future directions. *science* **2007**, *315* (5812), 612-617.
18. Krishnamurthy, A.; Moore, J. K.; Mahowald, N.; Luo, C.; Doney, S. C.; Lindsay, K.; Zender, C. S., Impacts of increasing anthropogenic soluble iron and nitrogen deposition on ocean biogeochemistry. *Global Biogeochemical Cycles* **2009**, *23* (3).
19. Morel, F.; Price, N., The biogeochemical cycles of trace metals in the oceans. *Science* **2003**, *300* (5621), 944-947.

20. Berman-Frank, I.; Cullen, J. T.; Shaked, Y.; Sherrell, R. M.; Falkowski, P. G., Iron availability, cellular iron quotas, and nitrogen fixation in *Trichodesmium*. *Limnology and Oceanography* **2001**, *46* (6), 1249-1260.
21. Johnson, K. S.; Gordon, R. M.; Coale, K. H., What controls dissolved iron concentrations in the world ocean? *Marine Chemistry* **1997**, *57* (3), 137-161.
22. Sohm, J. A.; Webb, E. A.; Capone, D. G., Emerging patterns of marine nitrogen fixation. *Nature Reviews Microbiology* **2011**, *9* (7), 499-508.
23. Hassler, C. S.; Alasonati, E.; Nichols, C. M.; Slaveykova, V., Exopolysaccharides produced by bacteria isolated from the pelagic Southern Ocean—Role in Fe binding, chemical reactivity, and bioavailability. *Marine Chemistry* **2011**, *123* (1), 88-98.
24. Boukhalfa, H.; Crumbliss, A. L., Chemical aspects of siderophore mediated iron transport. *Biometals* **2002**, *15* (4), 325-339.
25. Kustka, A. B.; Jones, B. M.; Hatta, M.; Field, M. P.; Milligan, A. J., The influence of iron and siderophores on eukaryotic phytoplankton growth rates and community composition in the Ross Sea. *Marine Chemistry* **2015**, *173*, 195-207.
26. Dhungana, S.; Crumbliss, A. L., Coordination chemistry and redox processes in siderophore-mediated iron transport. *Geomicrobiology Journal* **2005**, *22* (3-4), 87-98.
27. Mawji, E.; Gledhill, M.; Milton, J. A.; Tarran, G. A.; Ussher, S.; Thompson, A.; Wolff, G. A.; Worsfold, P. J.; Achterberg, E. P., Hydroxamate siderophores: occurrence and importance in the Atlantic Ocean. *Environmental science & technology* **2008**, *42* (23), 8675-8680.
28. Velasquez, I. Characterization of siderophores in the Southern Ocean. University of Otago, 2011.
29. Macrellis, H. M.; Trick, C. G.; Rue, E. L.; Smith, G.; Bruland, K. W., Collection and detection of natural iron-binding ligands from seawater. *Marine Chemistry* **2001**, *76* (3), 175-187.
30. Amin, S. A.; Parker, M. S.; Armbrust, E. V., Interactions between diatoms and bacteria. *Microbiology and Molecular Biology Reviews* **2012**, *76* (3), 667-684.
31. Amin, S. A.; Green, D. H.; Hart, M. C.; Küpper, F. C.; Sunda, W. G.; Carrano, C. J., Photolysis of iron–siderophore chelates promotes bacterial–algal mutualism. *Proceedings of the National Academy of Sciences* **2009**, *106* (40), 17071-17076.
32. Maldonado, M. T.; Price, N. M.; PRICE, N.; PRICE, N., Nitrate regulation of Fe reduction and transport in Fe-limited *Thalassiosira oceanica*. *Limnology and Oceanography* **2000**, *45* (4), 814-826.
33. Hassler, C.; Schoemann, V., Bioavailability of organically bound Fe to model phytoplankton of the Southern Ocean. *Biogeosciences* **2009**, *6* (10), 2281-2296.
34. Strzepek, R. F.; Maldonado, M. T.; Hunter, K. A.; Frew, R. D.; Boyd, P. W., Adaptive strategies by Southern Ocean phytoplankton to lessen iron limitation: Uptake of organically complexed iron and reduced cellular iron requirements. *Limnology and Oceanography* **2011**, *56* (6), 1983-2002.
35. Wells, M. L.; Trick, C. G., Controlling iron availability to phytoplankton in iron-replete coastal waters. *Marine chemistry* **2004**, *86* (1), 1-13.
36. McCormack, P.; Worsfold, P. J.; Gledhill, M., Separation and detection of siderophores produced by marine bacterioplankton using high-performance liquid chromatography with electrospray ionization mass spectrometry. *Analytical chemistry* **2003**, *75* (11), 2647-2652.
37. Butler, A.; Theisen, R. M., Iron (III)–siderophore coordination chemistry: reactivity of marine siderophores. *Coordination chemistry reviews* **2010**, *254* (3), 288-296.

38. Leslie, A. D.; Daneshfar, R.; Volmer, D. A., Infrared multiphoton dissociation of the siderophore enterobactin and its Fe (III) complex. Influence of Fe (III) binding on dissociation kinetics and relative energetics. *Journal of the American Society for Mass Spectrometry* **2007**, *18* (4), 632-641.
39. Karger, B. L.; Gant, J. R.; Martkopf, A.; Weiner, P. H., Hydrophobic effects in reversed-phase liquid chromatography. *Journal of Chromatography A* **1976**, *128* (1), 65-78.
40. Moberg, M. Liquid Chromatography Coupled to Mass Spectroscopy. Implementation of Chemometric Optimization and Selected Applications. . Uppsala University 2006.
41. Kristensen, D. B.; Imamura, K.; Miyamoto, Y.; Yoshizato, K., Mass spectrometric approaches for the characterization of proteins on a hybrid quadrupole time - of - flight (Q - TOF) mass spectrometer. *Electrophoresis* **2000**, *21* (2), 430-439.
42. Guilhaus, M., Special feature: Tutorial. Principles and instrumentation in time - of - flight mass spectrometry. Physical and instrumental concepts. *Journal of Mass Spectrometry* **1995**, *30* (11), 1519-1532.
43. Plumb, R. S.; Johnson, K. A.; Rainville, P.; Smith, B. W.; Wilson, I. D.; Castro - Perez, J. M.; Nicholson, J. K., UPLC/MSE; a new approach for generating molecular fragment information for biomarker structure elucidation. *Rapid Communications in Mass Spectrometry* **2006**, *20* (13), 1989-1994.
44. Velasquez, I.; Nunn, B. L.; Ibisani, E.; Goodlett, D. R.; Hunter, K. A.; Sander, S. G., Detection of hydroxamate siderophores in coastal and Sub-Antarctic waters off the South Eastern Coast of New Zealand. *Marine Chemistry* **2011**, *126* (1), 97-107.
45. Mohamed, K. N.; Gledhill, M., Determination of Specific Iron Chelator by Using LC-ICP-MS and LC-ESI-MS. *Procedia Environmental Sciences* **2015**, *30*, 256-261.
46. Mawji, E.; Gledhill, M.; Milton, J. A.; Zubkov, M. V.; Thompson, A.; Wolff, G. A.; Achterberg, E. P., Production of siderophore type chelates in Atlantic Ocean waters enriched with different carbon and nitrogen sources. *Marine Chemistry* **2011**, *124* (1), 90-99.
47. Price, N. M., Harrison, Gail I., Hering, Janet G., Hudson, Robert J., Nirel, Pascale, M.V., Palenik, Brian, Morel, Francois, M.M., Preparation and Chemistry of the Artificial Algal Culture Medium Aquil. *Biological Oceanography* **1989**, *6*, 443-461.
48. Lutz, V., Sathyendaranath, Shubha, Head, Erica, Li, William, Changes in the in vivo absorption and fluorescence excitation spectra with growth irradiance in three species of phytoplankton. *Journal of Plankton Research* **2001**, *23* (6), 555-569.
49. Dittmar, T., Koch, Boris, Norbert, Hertkorn, Kattner, Gerhard, A simple and efficient method for the solid-phase extraction of dissolved organic matter (SPE-DOM) from seawater *Limnol. Oceanogr.: Methods* **2008**, *6*, 230-235.
50. Waters. Progenesis QI User Guide: analysis workflow guidelines.
51. Alsberg, B. K., Chemometrics (Compendium for TKJ4175/KJ8175). NTNU: 2014.
52. Winkelmann, G.; Busch, B.; Hartmann, A.; Kirchhof, G.; Süßmuth, R.; Jung, G., Degradation of desferrioxamines by *Azospirillum irakense*: Assignment of metabolites by HPLC/electrospray mass spectrometry. *Biometals* **1999**, *12* (3), 255-264.
53. Pierwola, A.; Krupinski, T.; Zalupski, P.; Chiarelli, M.; Castignetti, D., Degradation pathway and generation of monohydroxamic acids from the trihydroxamate siderophore deferrioxamine B. *Applied and environmental microbiology* **2004**, *70* (2), 831-836.
54. Hotta, K.; Saito, N.; Okami, Y., Studies on new aminoglycoside antibiotics, istamycins, from an actinomycete isolated from a marine environment. I. The use of

plasmid profiles in screening antibiotic-producing streptomycetes. *The Journal of antibiotics* **1980**, *33* (12), 1502-1509.

55. Groenewold, G. S.; Van Stipdonk, M. J.; Gresham, G. L.; Chien, W.; Bulleigh, K.; Howard, A., Collision - induced dissociation tandem mass spectrometry of desferrioxamine siderophore complexes from electrospray ionization of UO_2^{2+} , Fe^{3+} and Ca^{2+} solutions. *Journal of mass spectrometry* **2004**, *39* (7), 752-761.

56. Villiers, M.; Barnard, L.; Koekemoer, L.; Snoep, J. L.; Strauss, E., Variation in pantothenate kinase type determines the pantothenamide mode of action and impacts on coenzyme A salvage biosynthesis. *FEBS Journal* **2014**, *281* (20), 4731-4753.

57. Öztürk, M.; Croot, P. L.; Bertilsson, S.; Abrahamsson, K.; Karlson, B.; David, R.; Fransson, A.; Sakshaug, E., Iron enrichment and photoreduction of iron under UV and PAR in the presence of hydroxycarboxylic acid: implications for phytoplankton growth in the Southern Ocean. *Deep Sea Research Part II: Topical Studies in Oceanography* **2004**, *51* (22), 2841-2856.

58. Fischbach, M. A.; Lin, H.; Liu, D. R.; Walsh, C. T., How pathogenic bacteria evade mammalian sabotage in the battle for iron. *Nature chemical biology* **2006**, *2* (3), 132-138.

59. Wishart, D. S.; Jewison, T.; Guo, A. C.; Wilson, M.; Knox, C.; Liu, Y.; Djoumbou, Y.; Mandal, R.; Aziat, F.; Dong, E., HMDB 3.0—the human metabolome database in 2013. *Nucleic acids research* **2012**, gks1065.

60. Pecoraro, V. L.; Harris, W. R.; Wong, G. B.; Carrano, C. J.; Raymond, K. N., Coordination chemistry of microbial iron transport compounds. 23. Fourier transform infrared spectroscopy of ferric catechoylamide analogues of enterobactin. *Journal of the American Chemical Society* **1983**, *105* (14), 4623-4633.

61. Kraemer, H.-J.; Breithaupt, H., Quantification of desferrioxamine, ferrioxamine and aluminoxamine by post-column derivatization high-performance liquid chromatography: Non-linear calibration resulting from second-order reaction kinetics. *Journal of Chromatography B: Biomedical Sciences and Applications* **1998**, *710* (1), 191-204.

62. Meyer, A.; Höffler, S.; Fischer, K., Anion-exchange chromatography–electrospray ionization mass spectrometry method development for the environmental analysis of aliphatic polyhydroxy carboxylic acids. *Journal of Chromatography A* **2007**, *1170* (1), 62-72.

Appendix

DFB Series

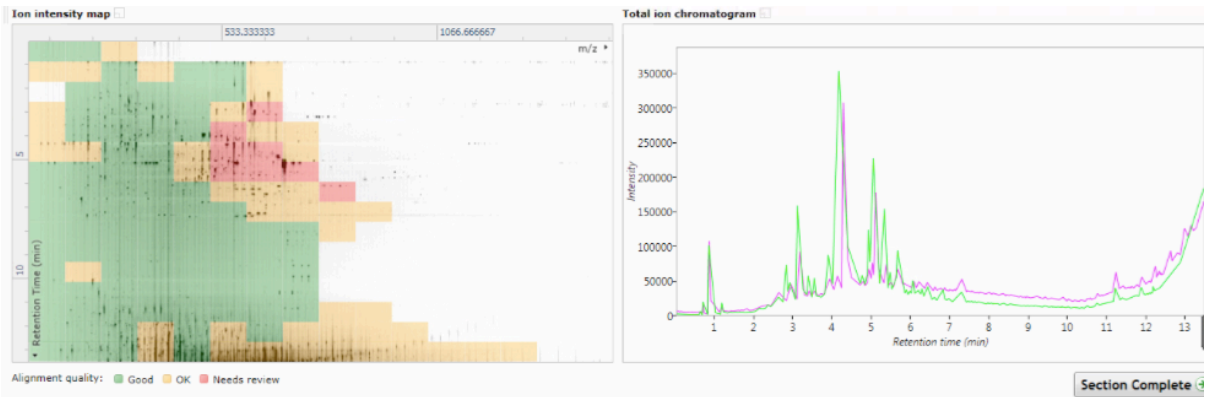


Figure A.1. Alignment issues around DFB retention time and m/z as shown by the red in the ion intensity map for a 10000 nM experimental sample.

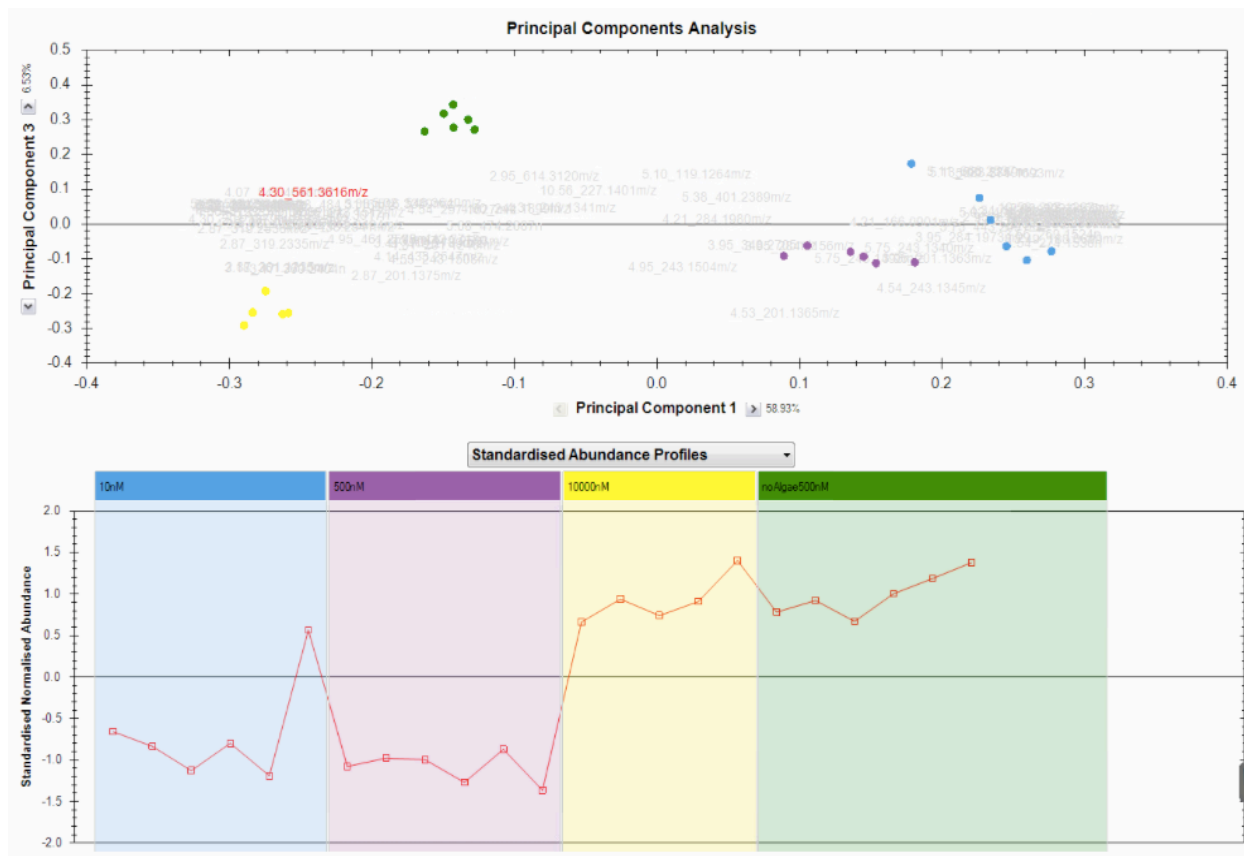


Figure A.2. PCA comparing PC 1 and 3 along with the abundance profile for DFB

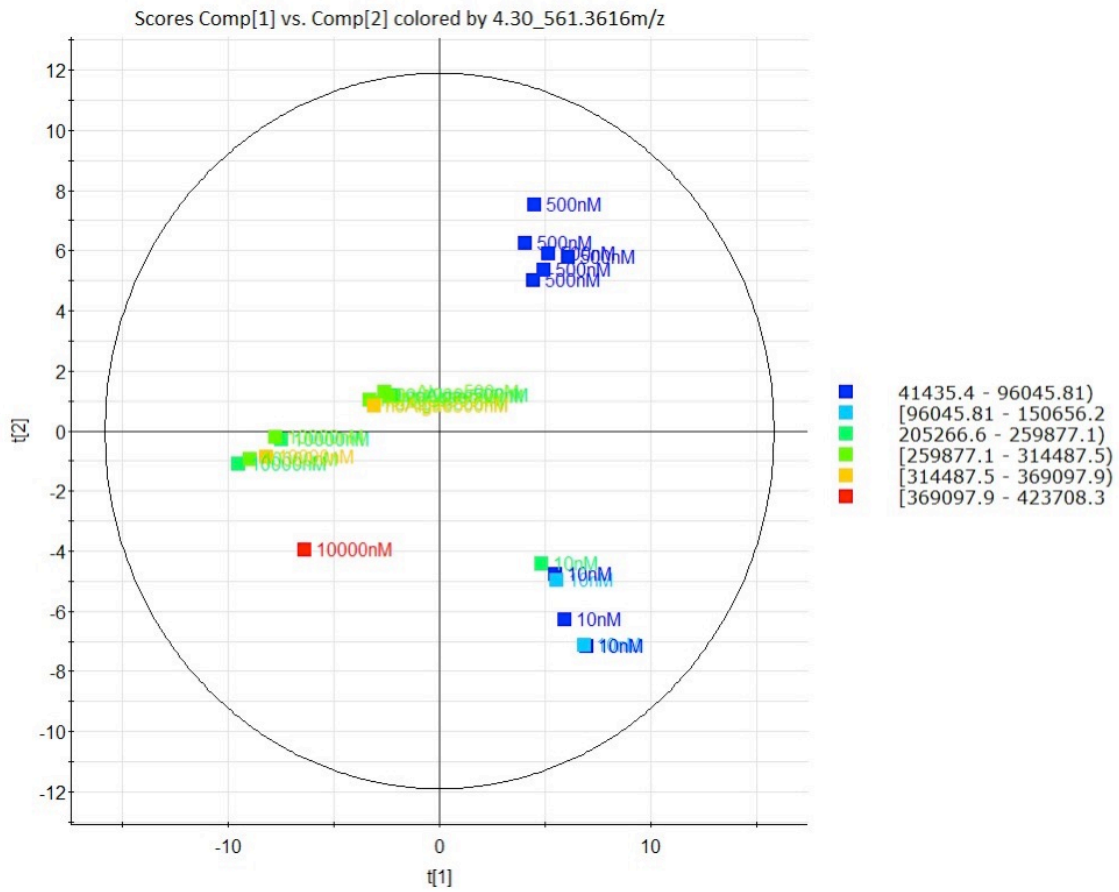


Figure A.3. Scores plot for PC 1 and 2 showing the conditions in the DFB series with colors corresponding to the abundance of DFB.

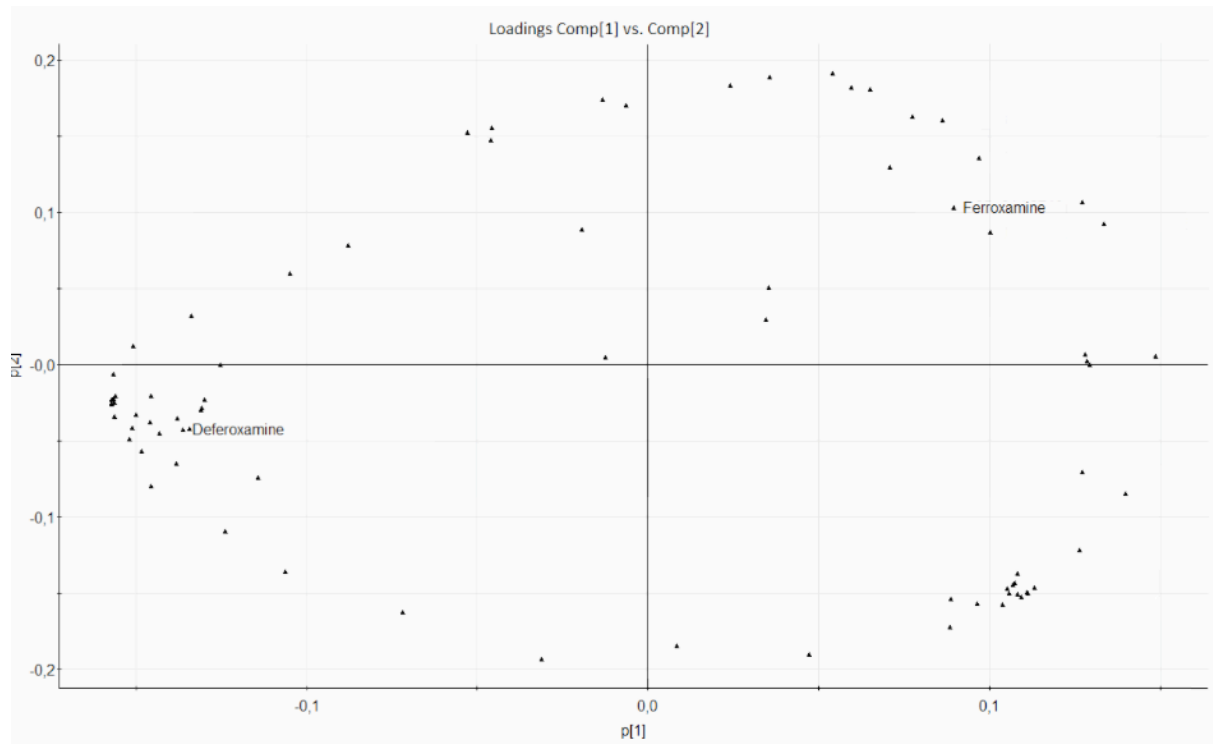


Figure A.4. Loadings plot for PC 1 and 2 with DFB and ferrioxamine identified.

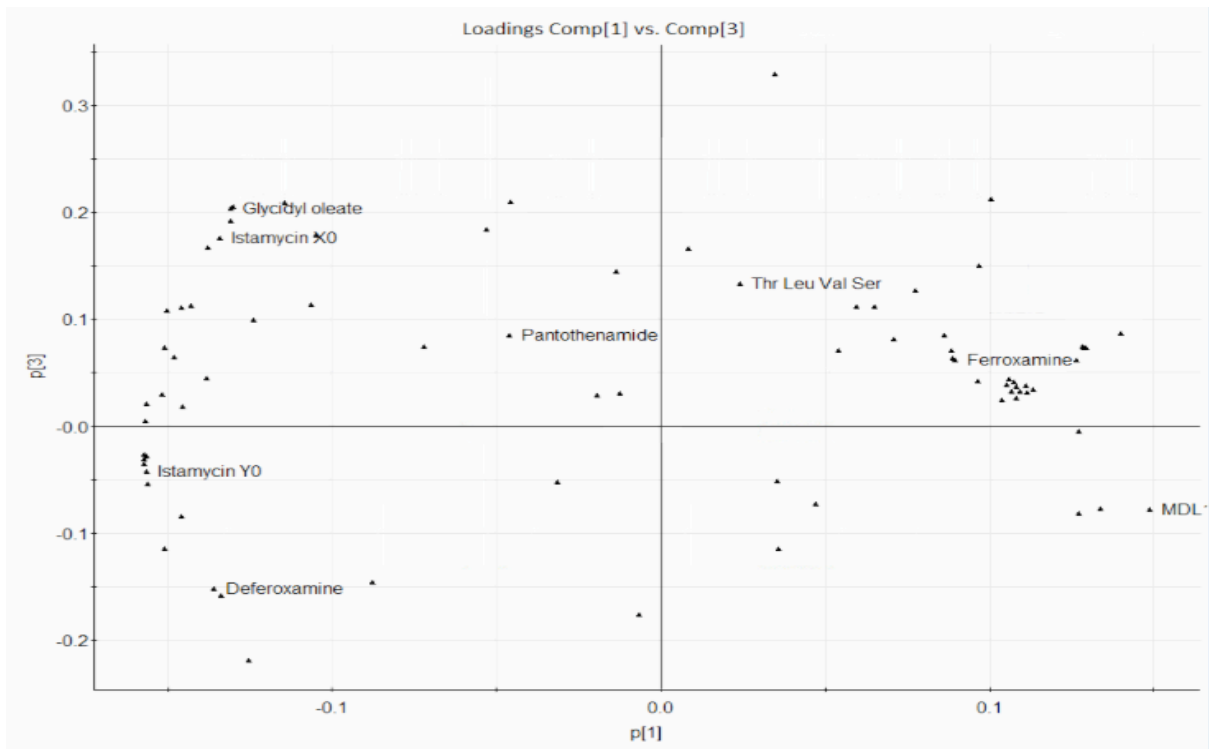


Figure A.5. Loadings plot for PC 1 and 3 with identified compounds.

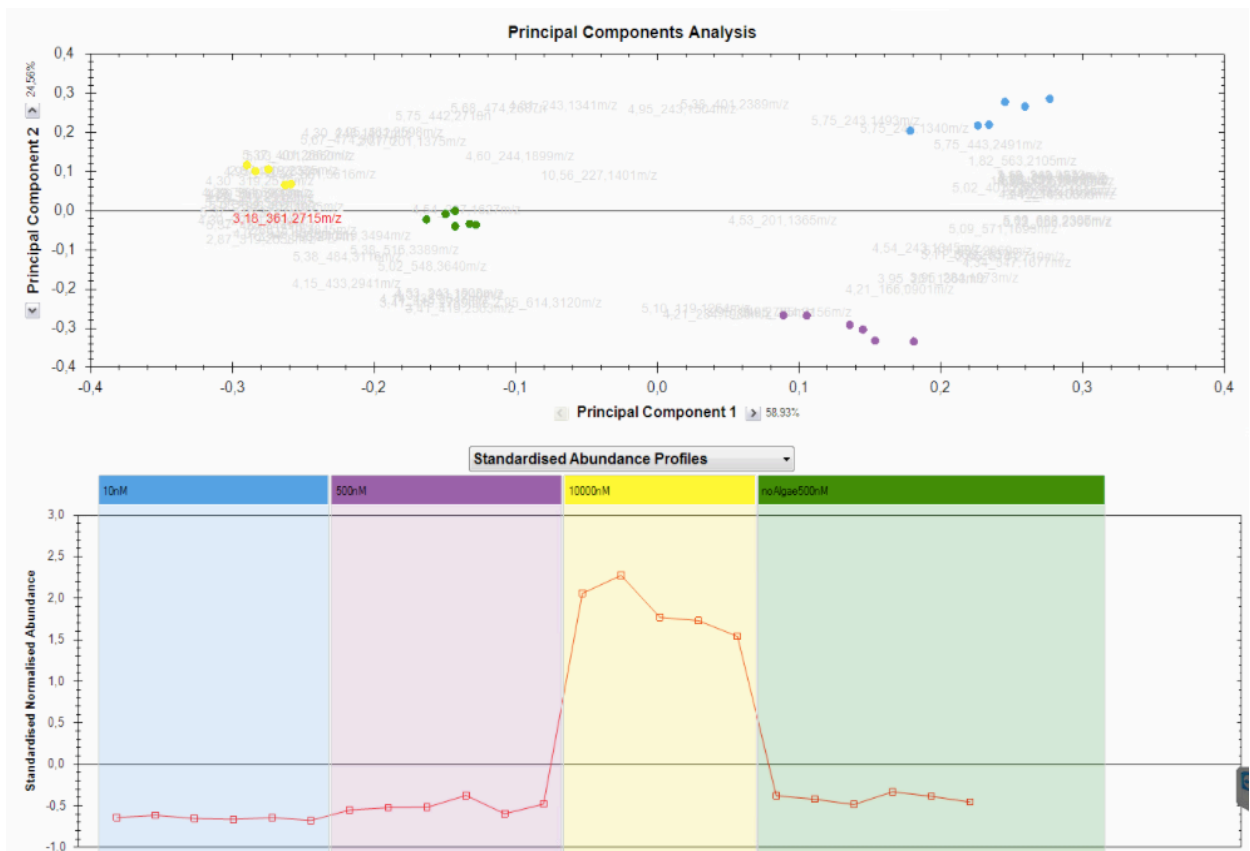


Figure A.6. PCA and abundance profile for 3.61_361.2715m/z.

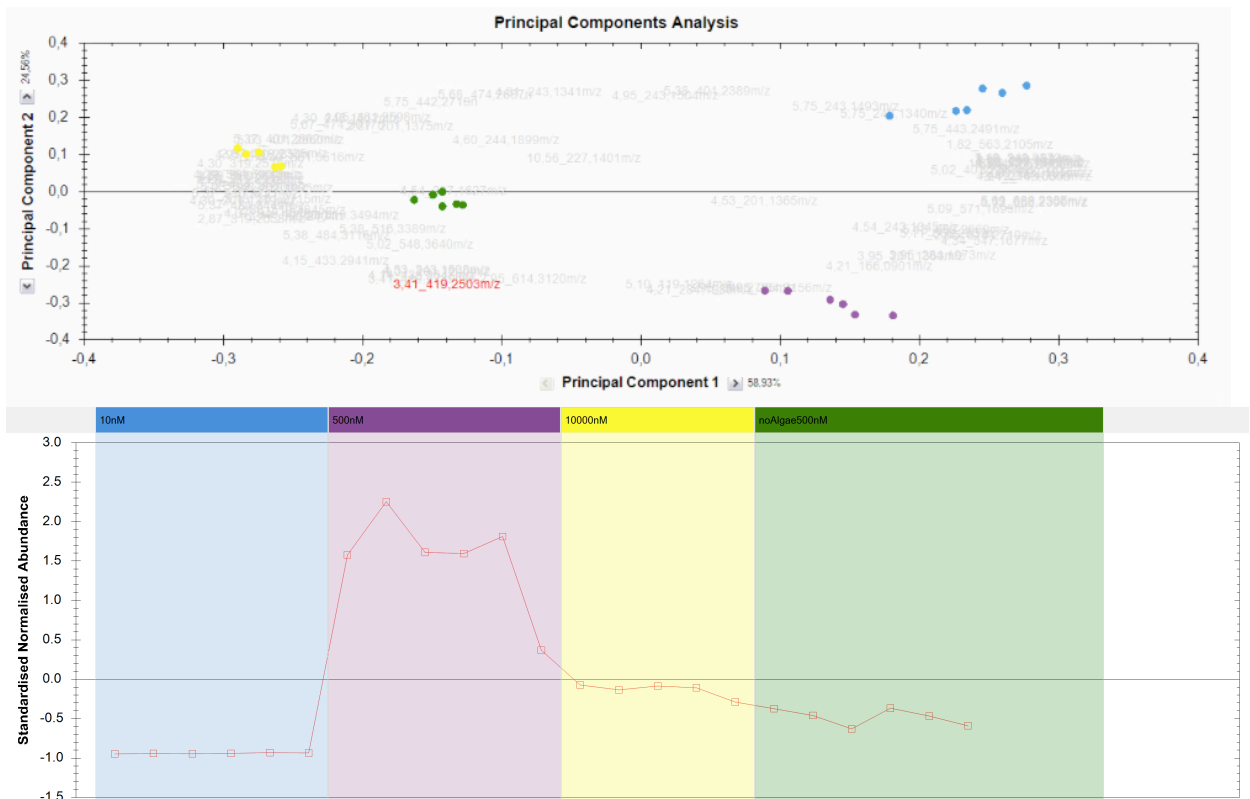


Figure A.7. PCA and abundance profile for 3.41_419.2503m/z.

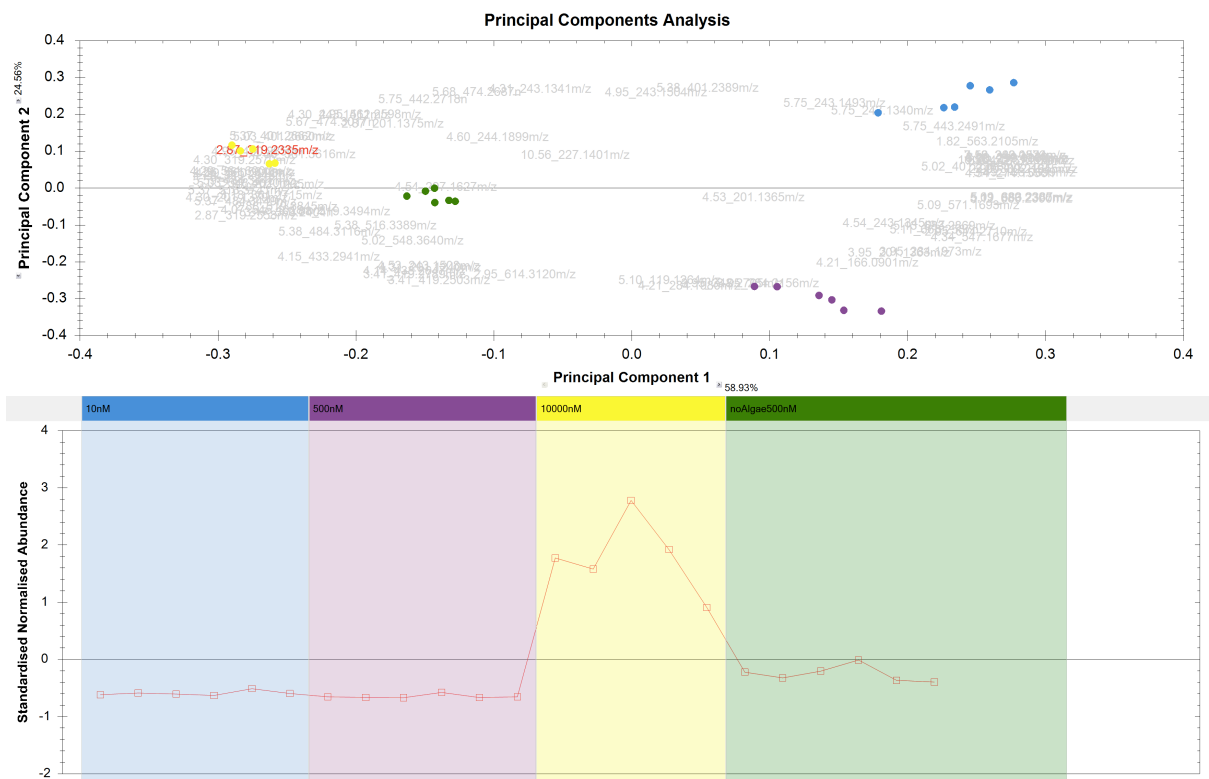


Figure A.8. PCA and abundance profile for 2.87_319.2335m/z.

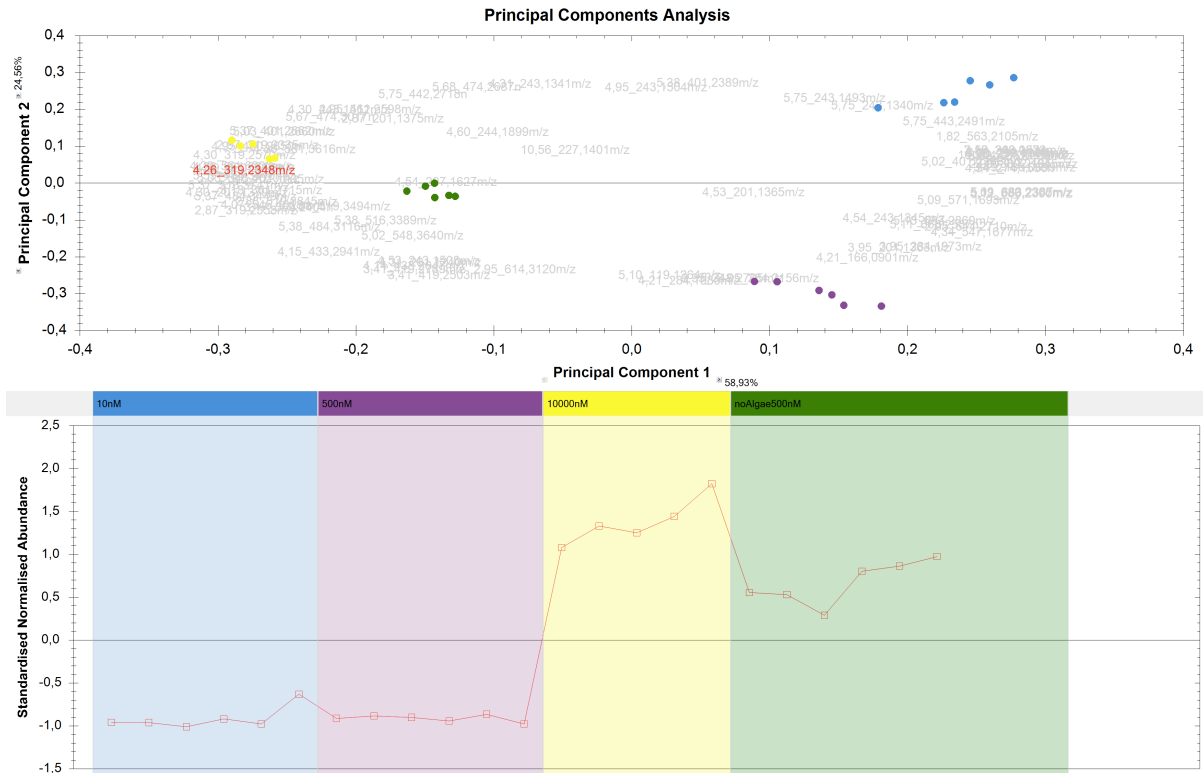


Figure A.9. PCA and abundance profile for 4.26_319.2348m/z.

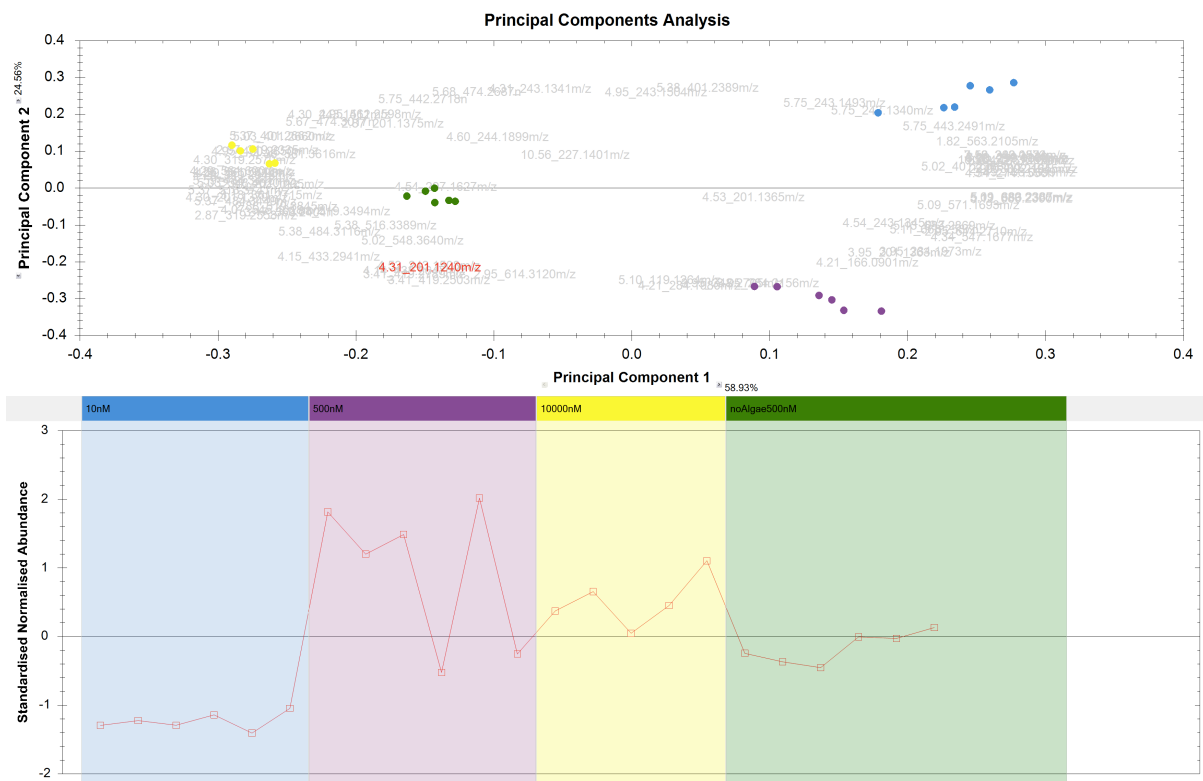


Figure A.10. PCA and abundance profile for 4.31_201.1240m/z.

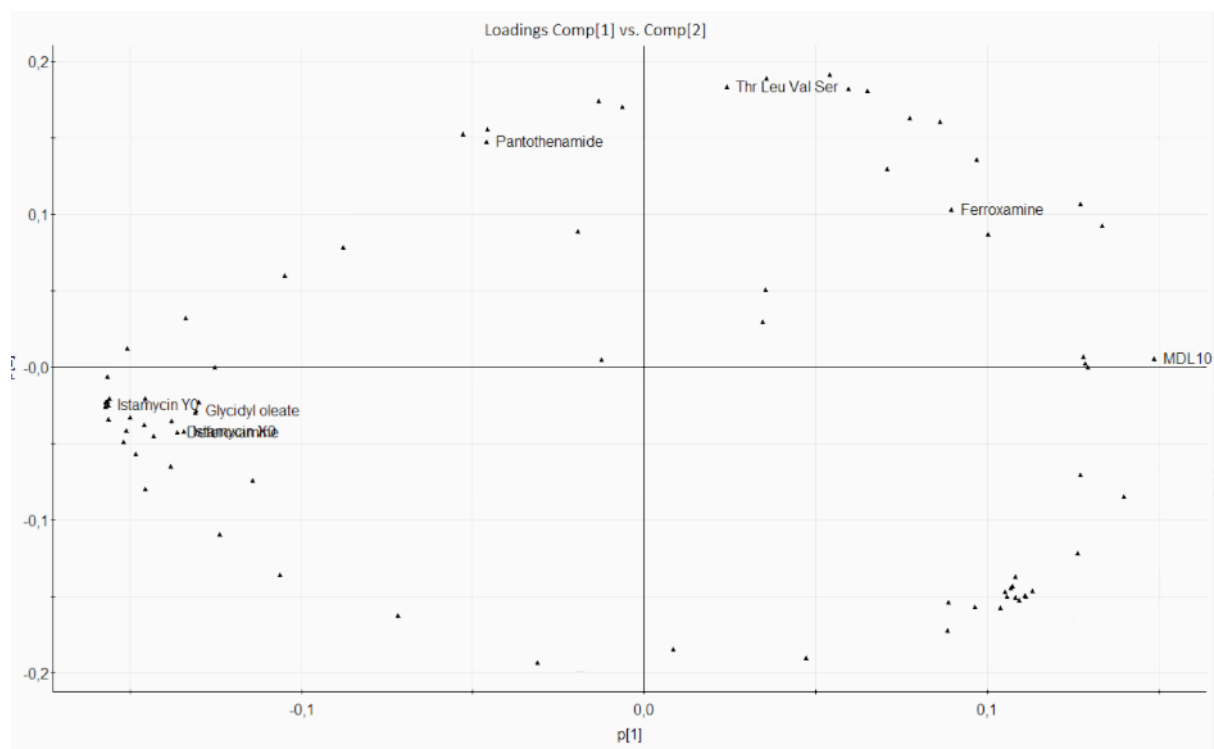


Figure A.14. Loadings plot showing the DFB, ferrioxamine, and discussed compounds. *

* Glycidyl oleate corresponds to 3.18_361.2715m/z. Thr Leu Val Ser corresponds to 3.41_419.2503m/z. Istamycin Y0 corresponds to 2.87_319.2335m/z and 4.26_319.2348m/z, one of which overlaps with Deferoxamine. Pantothenamamide corresponds to 4.31_201.1240m/z. MDL10 corresponds to the glucuronide at 5.09_571.1693m/z.

Enterobactin Series

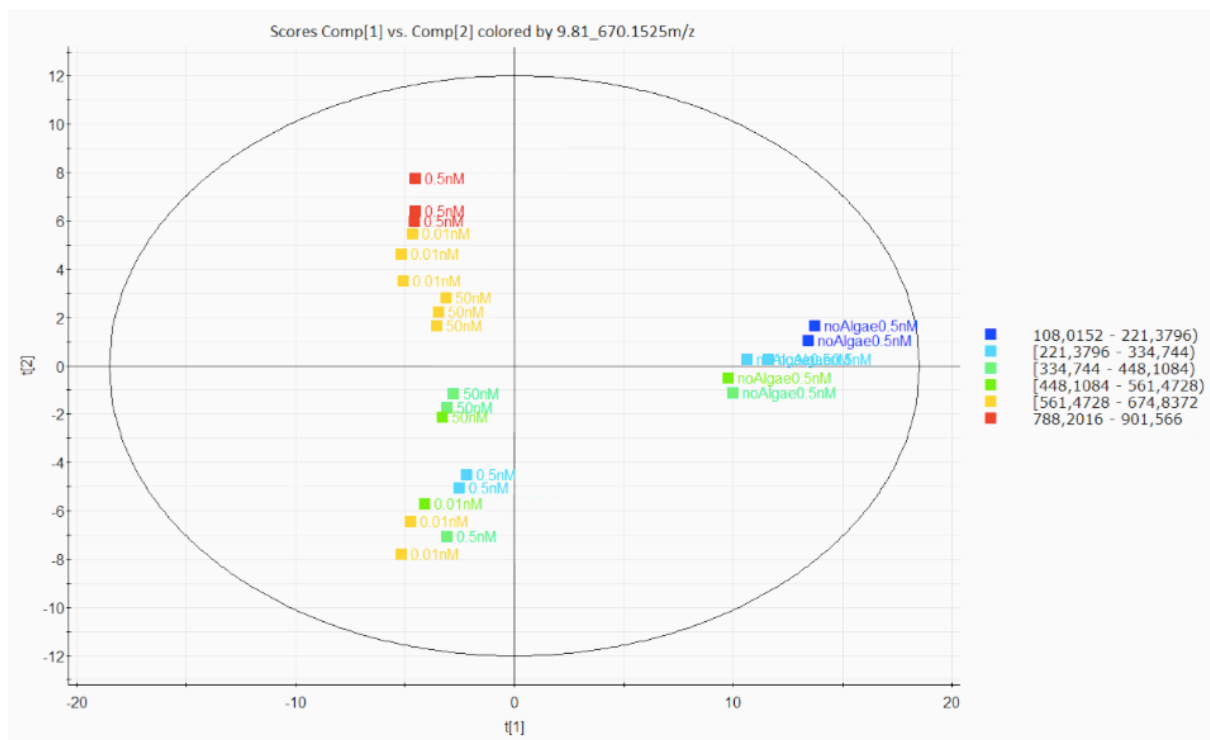


Figure A.15. Scores plot for PC 1 and 2 showing the conditions in the enterobactin series with colors corresponding to the abundance of enterobactin

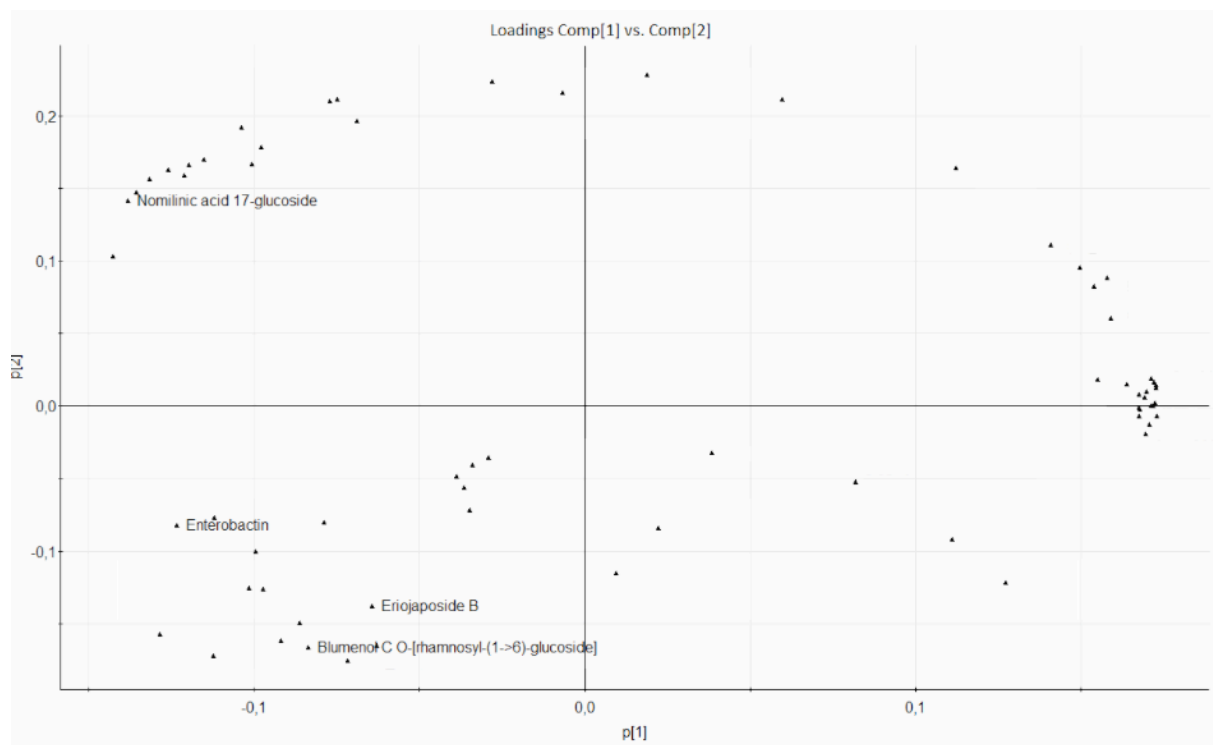


Figure A.16. Loadings plot for PC 1 and 2 showing enterobactin and other discussed compounds.

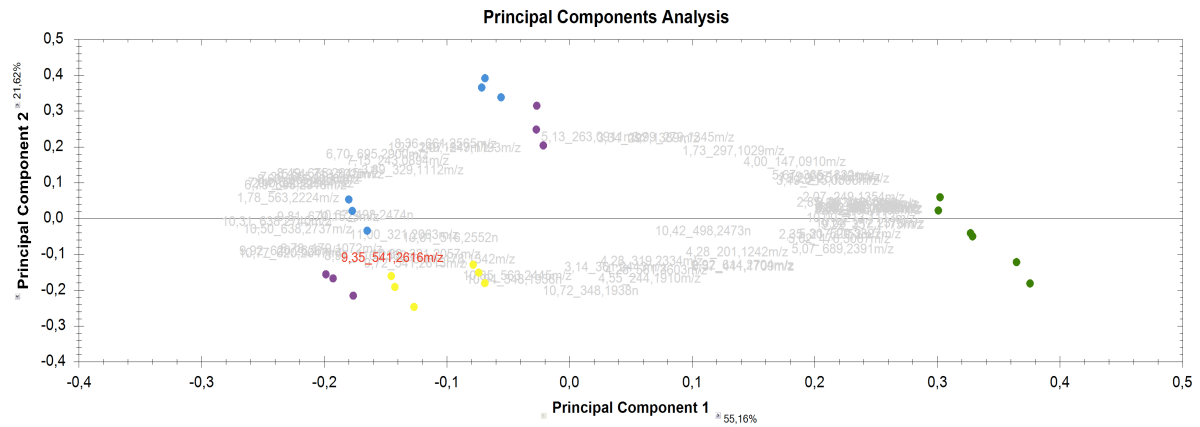


Figure A.17. PCA highlighting 9.35_541.2616m/z identified as a blumenol glucoside. *

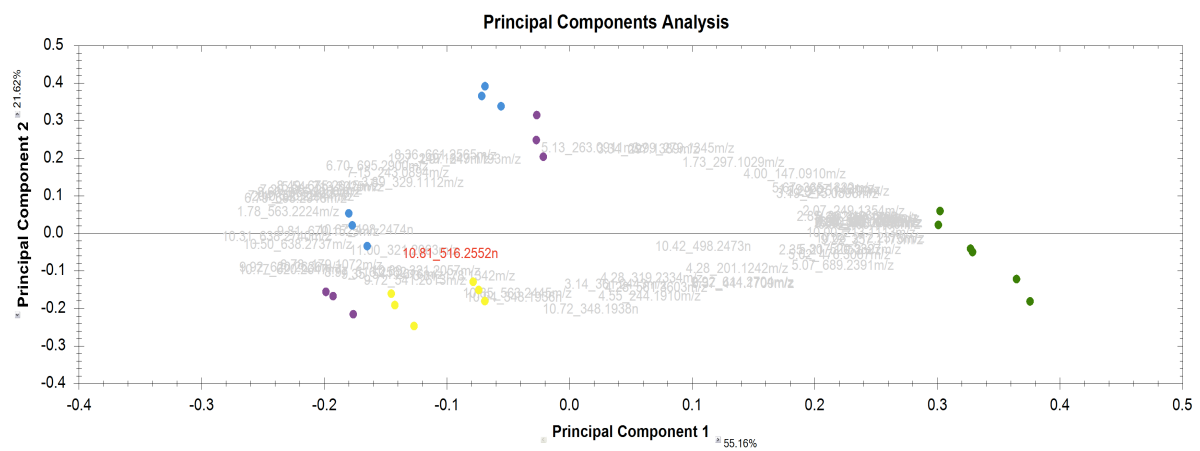


Figure A.18. PCA highlighting 10.15_516.2552m/z identified as a eriojaposide B. *

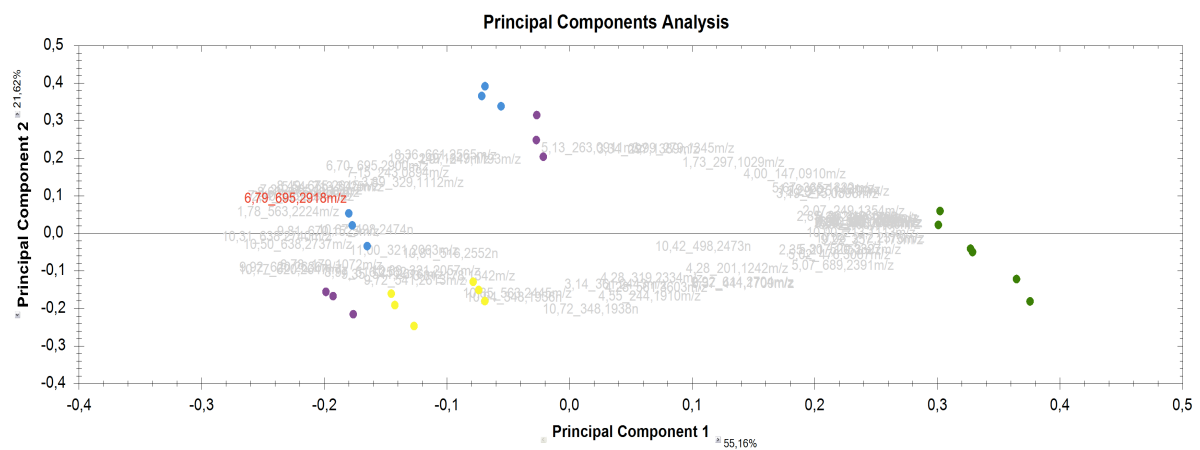


Figure A.19. PCA highlighting 6.79_695.2918m/z identified as a nomilinic acid 17-glucoside. *

*Purple matches the 0.1 nM condition, blue the 0.5 nM condition, yellow the 50 nM condition, and green the 0.5 nM, no algae condition.